THE UNIVERSITY OF MICHIGAN
ANN ARBOR, MICHIGAN

SEMIANNUAL PROGRESS REPORT NO. 11

ON

MICROWAVE DEVICE INVESTIGATIONS

This report covers the period October 1, 1971 to April 1, 1972

Electron Physics Laboratory
Department of Electrical and Computer Engineering

By: K. K. Dutta Choudhury
      G. I. Haddad
      S. P. Kwok
      N. A. Masnari
      R. J. Trew

Approved by: _G. I. Haddad_

G. I. Haddad, Director
Electron Physics Laboratory

Project 084000

May, 1972

TABLE OF CONTENTS

LIST OF ILLUSTRATIONS

LIST OF TABLES

PUBLICATIONS DURING THE LAST PERIOD

M. S. Gupta and R. J. Lomax, "Injection Locking in IMPATT Diode Oscillators," Proc. Third Biennial Cornell Electrical Engineering Conf., Ithaca, New York, pp. 215-223, August 1971.

I. I. Eldumiati and G. I. Haddad, "Effect of Magnetic Field on the Performance of Millimeter-Wave Detectors Using Bulk InSb," IEEE Trans. on Electron Devices (submitted for publication).

I. I. Eldumiati and G. I. Haddad, "Microwave Properties of n-Type InSb in a Magnetic Field Between 4 and 300°K," J. Appl. Phys. (to be published).

R. J. Trew, N. A. Masnari and G. I. Haddad, "Intermodulation Characteristics of X-Band IMPATT Amplifiers," To be presented at the 1972 IEEE-GMTT Int. Microwave Symp., Chicago, Ill., May 1972.

SEMIANNUAL PROGRESS REPORT NO. 11

ON

MICROWAVE DEVICE INVESTIGATIONS

1. General Introduction   (G. I. Haddad)

The purpose of this program is to investigate materials, devices and novel schemes for generation, amplification and detection of microwave and millimeter-wave energy. Several tasks were active during this report period under this program. These include:

  1. Schottky-barrier microwave devices.

  2. Intermodulation products in IMPATT diode amplifiers.

  3. Harmonic generation using Read-diode varactors.

The work performed on these tasks is described in detail in the following sections of this report.

2. Punch-Through Semiconductor Microwave Devices

  Supervisor: G. I. Haddad

    Staff: S. P. Kwok

  2.1 Introduction. The purpose of this phase of the program is to investigate theoretically and experimentally the properties of punch-through microwave semiconductor devices. Devices of the pnp^+, metal-np^+ and metal-n-metal types have been fabricated and tested. A theoretical analysis of these devices is also being carried out.

  2.2 Device Fabrication.

    2.2.1 PtSi-np^+ Devices. The 10 Ω-cm epitaxial layer of an np^+ Si wafer is thinned to 10 μm by etching, and then the surface is Syton polished to a smooth finish. The substrate is then etched to 0.001 inch and rinsed

in TCE, acetone, HF, DI water and methanol. The n-epitaxial layer is then dc
backsputtered at 1500 V in an argon discharge and a current of 50 mA for
1 minute. The Pt target is bombarded for a few minutes before the wafer is
brought in to be sputtered. The n-epitaxial layer is sputtered for one-half
minute at 1000 V and 50 mA. The deposited Pt film was measured to be
approximately 100 $\mathring{A}$. (The actual measurement was made on a Pt film sputtered
under identical conditions for 2 minutes and the deposited film thickness
was found to be 400 $\mathring{A}$ on the average. The thickness measurement was done by
means of a thickness measuring probe.) The wafer is sintered in vacuum at
650°C for 10 minutes to form a PtSi interface. The wafer is then transferred
to an evaporation vacuum jar where it is baked at 300°C for 15 minutes and
cooled for the same period prior to depositions of Cr (200 $\mathring{A}$) and Au (3000 $\mathring{A}$)
layers on both sides. A gold layer of 0.001 inch thickness is then electro-
plated on the epitaxial layer side to provide a heat sink. Using standard
photolithographic techniques, 0.010 inch diameter diode patterns are formed.
The devices are obtained by etching from the p^+ side sequentially the Au, Cr,
Si, PtSi and Cr. The diodes are now separated but remain on the thick gold
pad. The metal overhang due to undercutting during etching and the residual
photoresist are removed by means of ultrasonic cleaning in acetone. The
diodes are dried in a 150°C oven for one hour or more and diced into 0.025
by 0.025 inch square chips. The diodes are mounted in a standard S4 package
using thermocompression bonding at 300°C. If the I-V characteristic is
acceptable, a cap is spot welded onto the package and the device is ready for
testing. A typical I-V characteristic of such devices is given in Fig. 2.1.

    2.2.2 <u>Cr-n-Cr Devices</u>. For these devices an nn^+ Si wafer with
7 to 11 Ω-cm epitaxial layer resistivity is employed. The n^+ substrate and
part of the epitaxial layer are etched until the material looks yellowish
brown. The corresponding thickness is approximately 10 μm. There is always

20 V/DIVISION
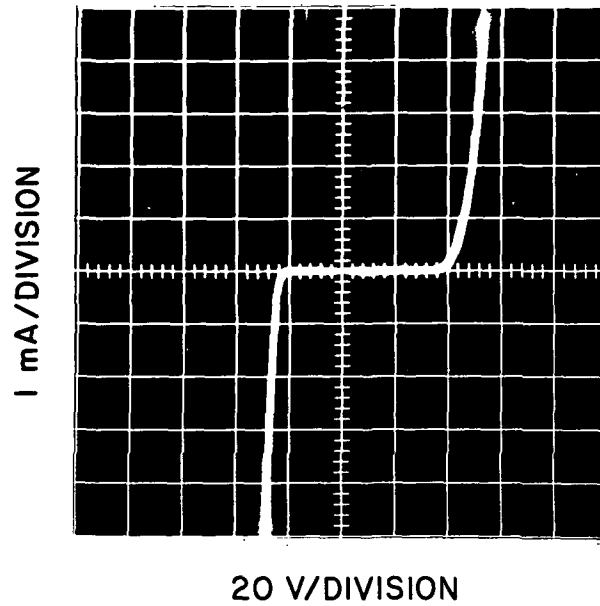
LEFT: SCHOTTKY-BARRIER REVERSE BIASED

FIG. 2.1 TYPICAL I-V CHARACTERISTIC OF PtSi-np$^+$ DIODE.

a considerable spread in the thicknesses with such a thinning process. The wafer is heated at 300°C in vacuum for one-half hour, and a Cr film (200 Å) is deposited on both sides of the wafer. The wafer is cooled for one-half hour and gold is evaporated (3000 Å) on both sides for making contacts. The separation of the diodes is done in the same manner described earlier. A typical I-V characteristic prior to thermocompression bonding is shown in Fig. 2.2, which looks promising. However, the devices become leaky after bonding, and no oscillation has been observed in such diodes yet.

2.2.3 pnp^+ Devices. An np^+ wafer identical with that described in Section 2.2.1 is used and again the epitaxial layer is thinned and cleaned as in the earlier case. A borosilicafilm II droplet was placed on the epitaxial layer and spun at 3000 rpm for 5 seconds. Boron diffusion is then made at 1020°C with 2400 cm^3/min nitrogen flow for 22.5 minutes. The unwanted boron doped oxide is removed by immersing the wafer in buffered HF for one minute. The measured surface resistance was approximately 13 Ω per square. The p^+ substrate is then thinned to 0.001 inch and cleaned in TCE, acetone, methanol, HF, DI water and methanol. The contact metallization, diode separation and packaging are done using the same procedure as that in the case of Section 2.2.1. A typical I-V characteristic of pnp^+ devices is shown in Fig. 2.3.

2.3 Experimental Characterization. The I-V characteristics of PtSi-np^+ at 300°K and 77°K are shown in Figs. 2.4 and 2.5, respectively. When the Schottky barrier is reverse biased the current level for each voltage is reduced for the 77°K case, which indicates the nonavalanche nature of the breakover characteristic. The only exception occurs at high currents (near 10 mA) where the current is lower for a high temperature. This is probably due to the increase in the series resistance at high temperature. For the case when the np^+ junction is reverse biased the currents at very high
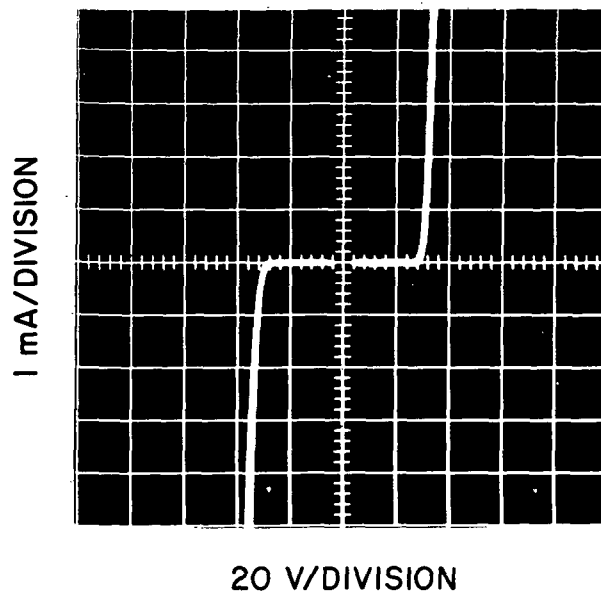
FIG. 2.2 TYPICAL I-V CHARACTERISTIC OF Cr-n-Cr DIODE.

I mA/DIVISION
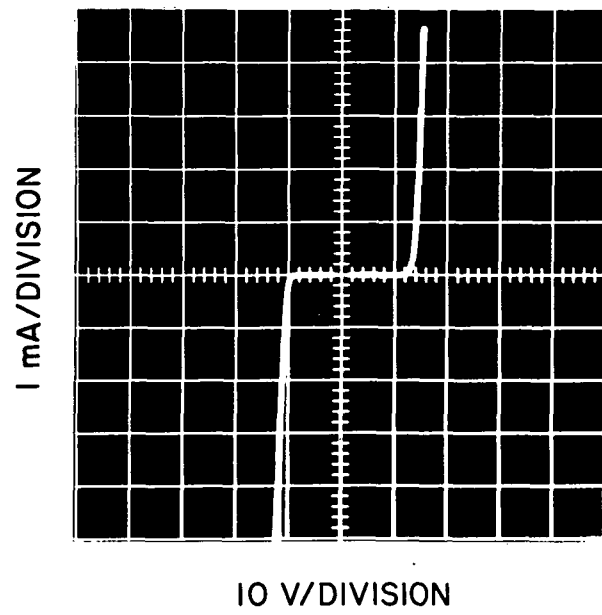
IO V/DIVISION

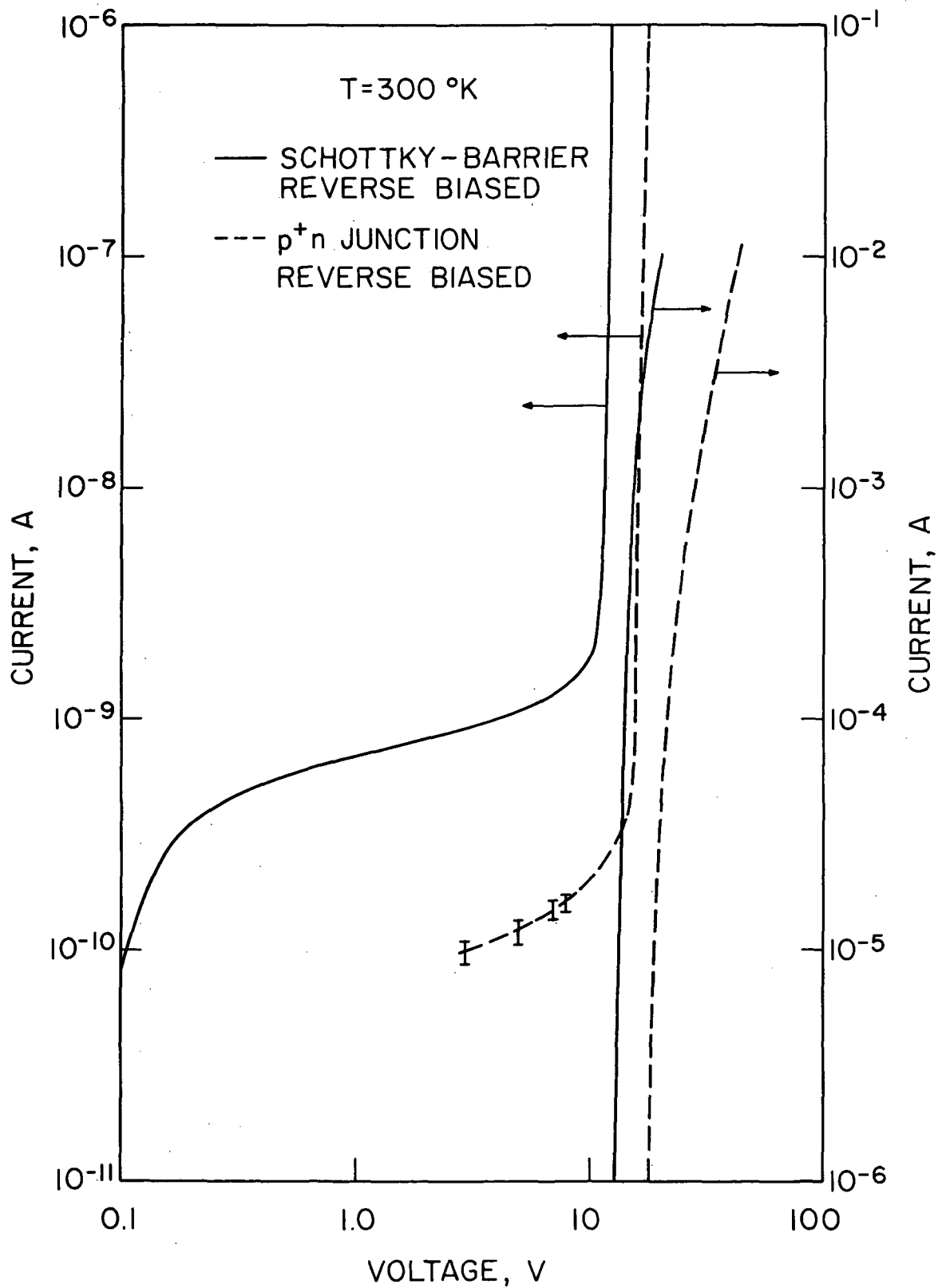FIG. 2.3 TYPICAL I-V CHARACTERISTIC OF pnp^+ DIODE.

FIG. 2.4 TYPICAL I-V CHARACTERISTIC OF PtSi-np$^+$ DIODES AT 300°K.
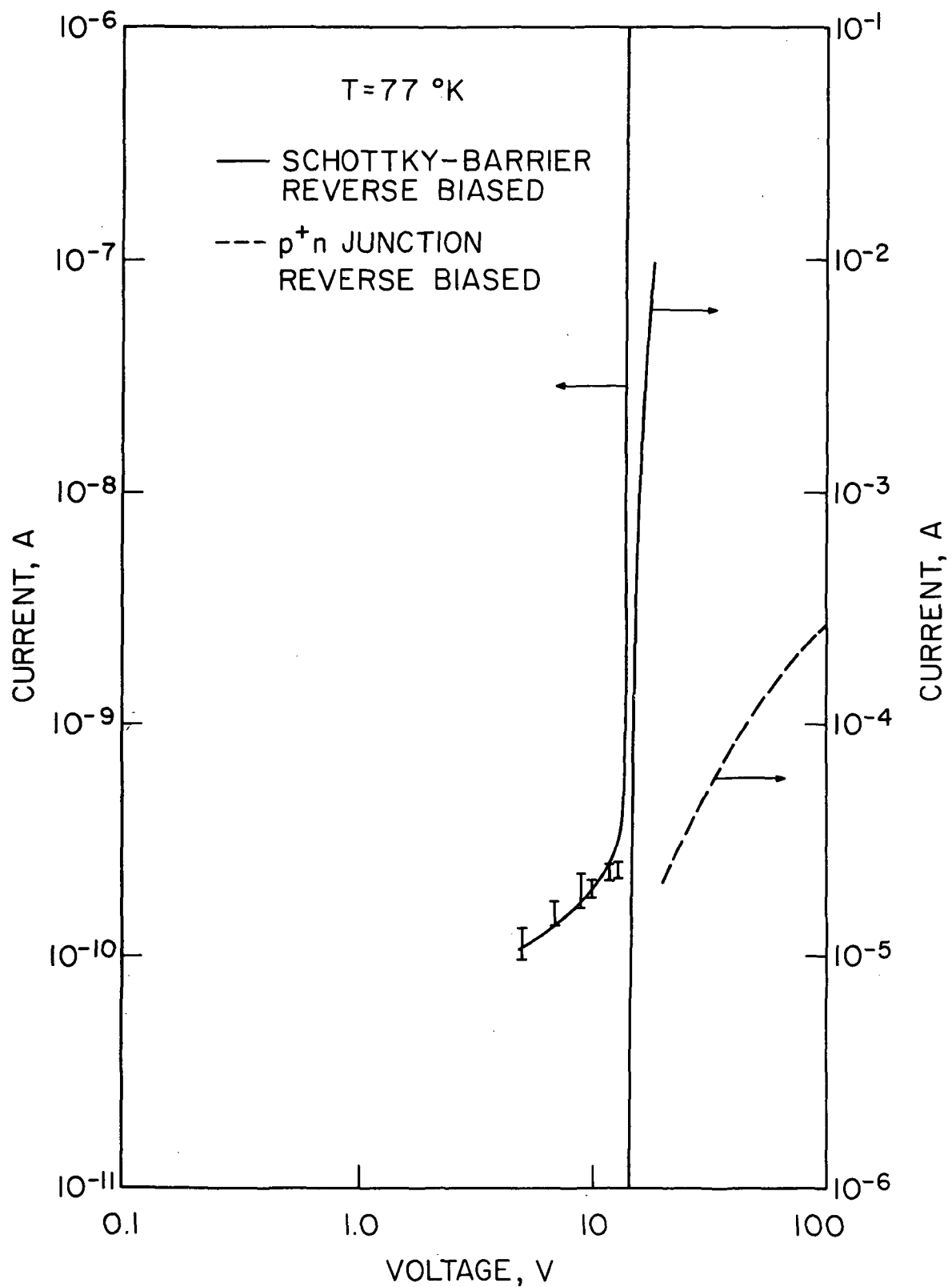
FIG. 2.5   TYPICAL I-V CHARACTERISTIC OF PtSi-np$^+$ DIODES AT 77°K.

voltages (greater than 20 V) are markedly reduced at 77°K, indicating the temperature-limited effect of the thermionic emission of the Schottky barrier. No microwave oscillation was observed in the group of devices having such an I-V characteristic. The I-V characteristic of the devices which generate microwave power is shown in Fig. 2.6. The device exhibits a dc negative resistance at current value near 10 mA when the p^+n junction is reverse biased; whereas no such negative resistance is observed when biased in the opposite polarity. Microwave oscillation occurs only in the former polarity, i.e., p^+n junction reverse biased. For these devices the maximum power occurs at a current level where dc negative resistance is observed, as shown in Fig. 2.7. The possibility of avalanching is ruled out due to the fact that at such polarity the current at 0°C shows the trend of temperature-limited thermionic emission as shown in Fig. 2.6. These devices oscillate in an S-band waveguide cavity incorporating a sliding short and a slide-screw tuner. The nominal frequency of oscillation was 4.6 GHz and the highest power output observed was 0.47 mW. Figure 2.7 shows the power vs. current plot of these devices. A Raytheon unit which yielded 1.5 mW at the same frequency in a coaxial cavity when placed in this circuit only delivered 0.42 mW. This indicates that the devices fabricated here might have the same level of power output. However, so far no oscillation has been observed with those devices placed in the coaxial cavity.

Oscillations are also observed in the pnp^+ devices placed in a 50-Ω coaxial cavity, the observed peak power output is 0.23 mW. Figure 2.8 shows the similar plots of power vs. bias current for a typical diode for different tuning slugs.

The low-noise characteristic of punch-through devices is exhibited in the narrow frequency spectrum of a PtSi-np^+ oscillator shown in Fig. 2.9.

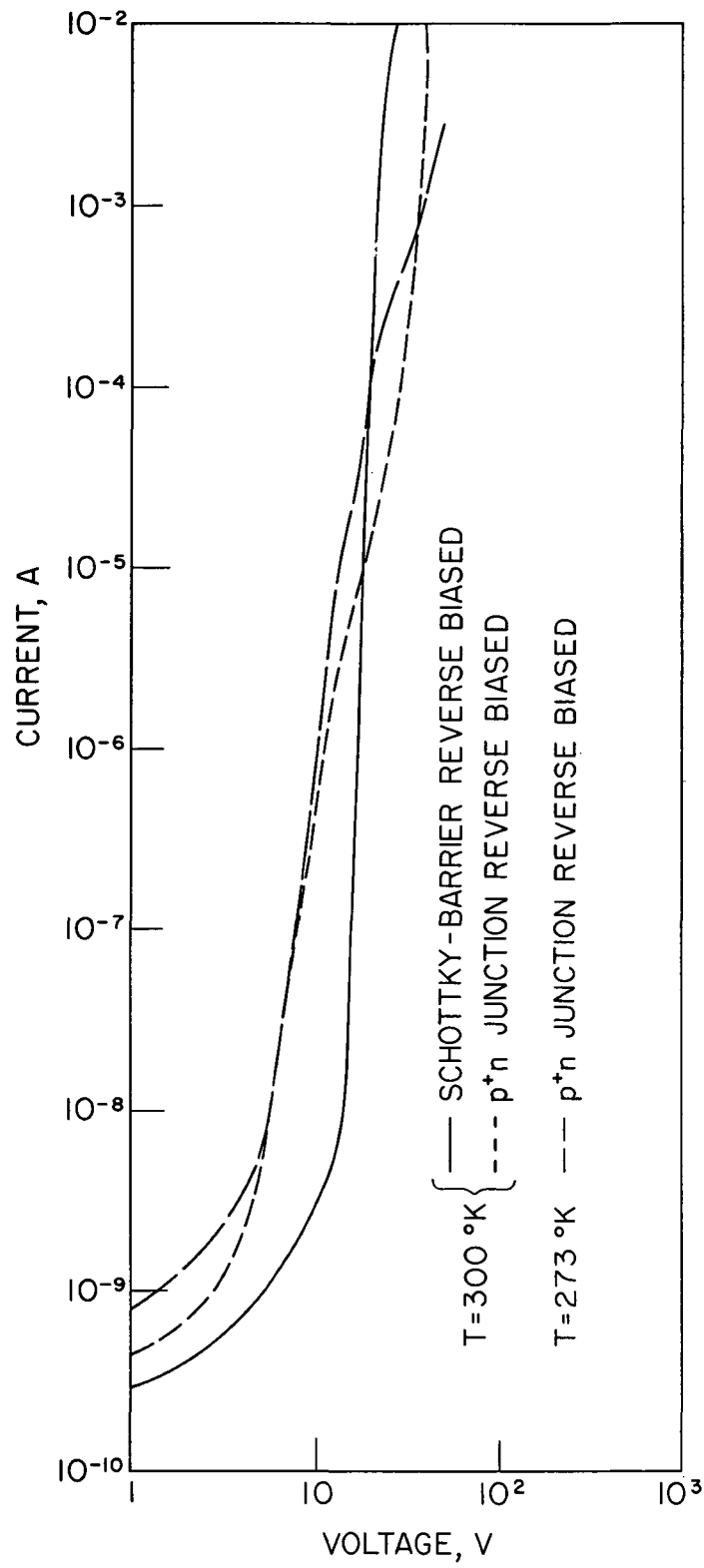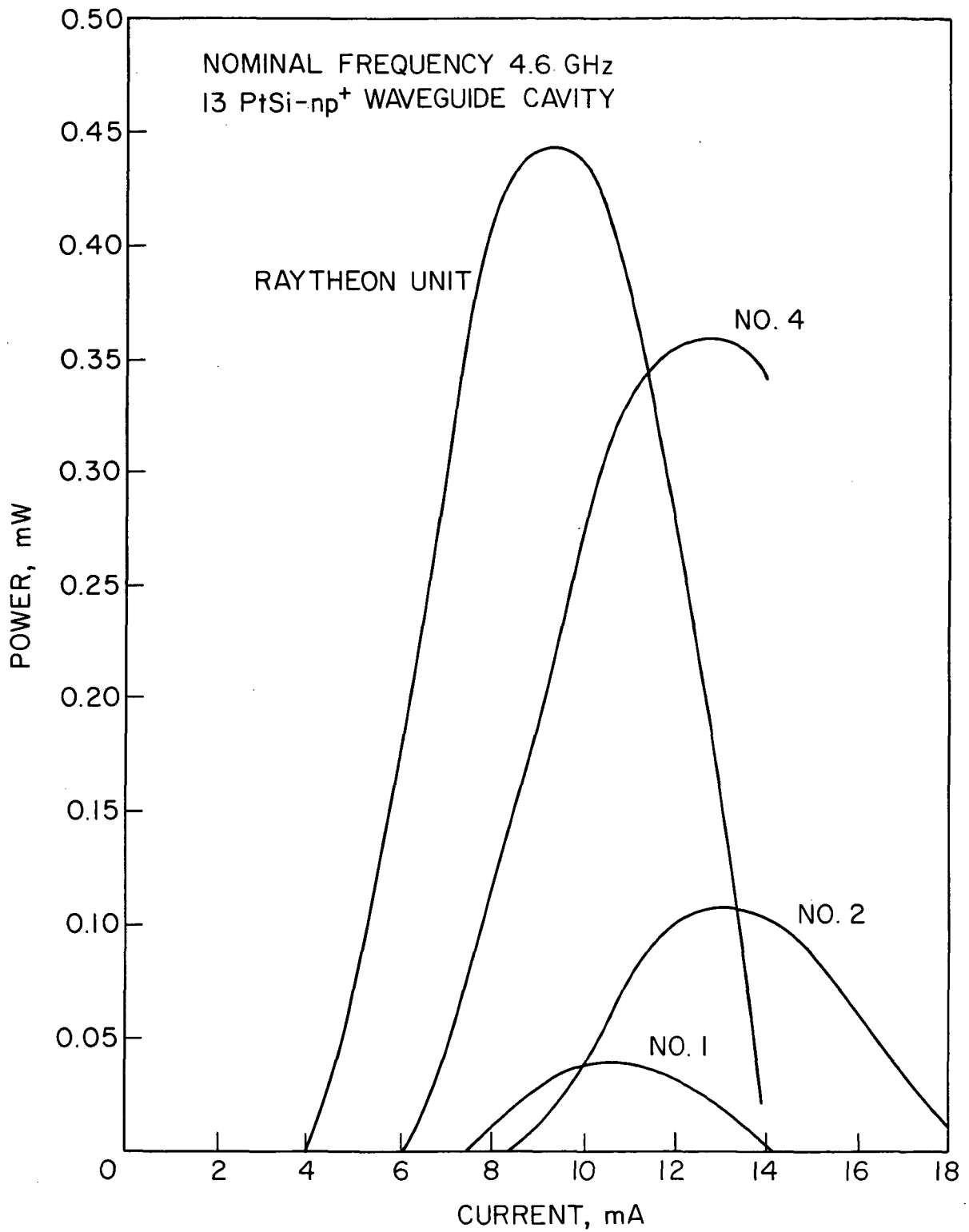FIG. 2.6 TYPICAL I-V CHARACTERISTIC OF PtSi-np$^+$ AT 300°K AND 273°K.

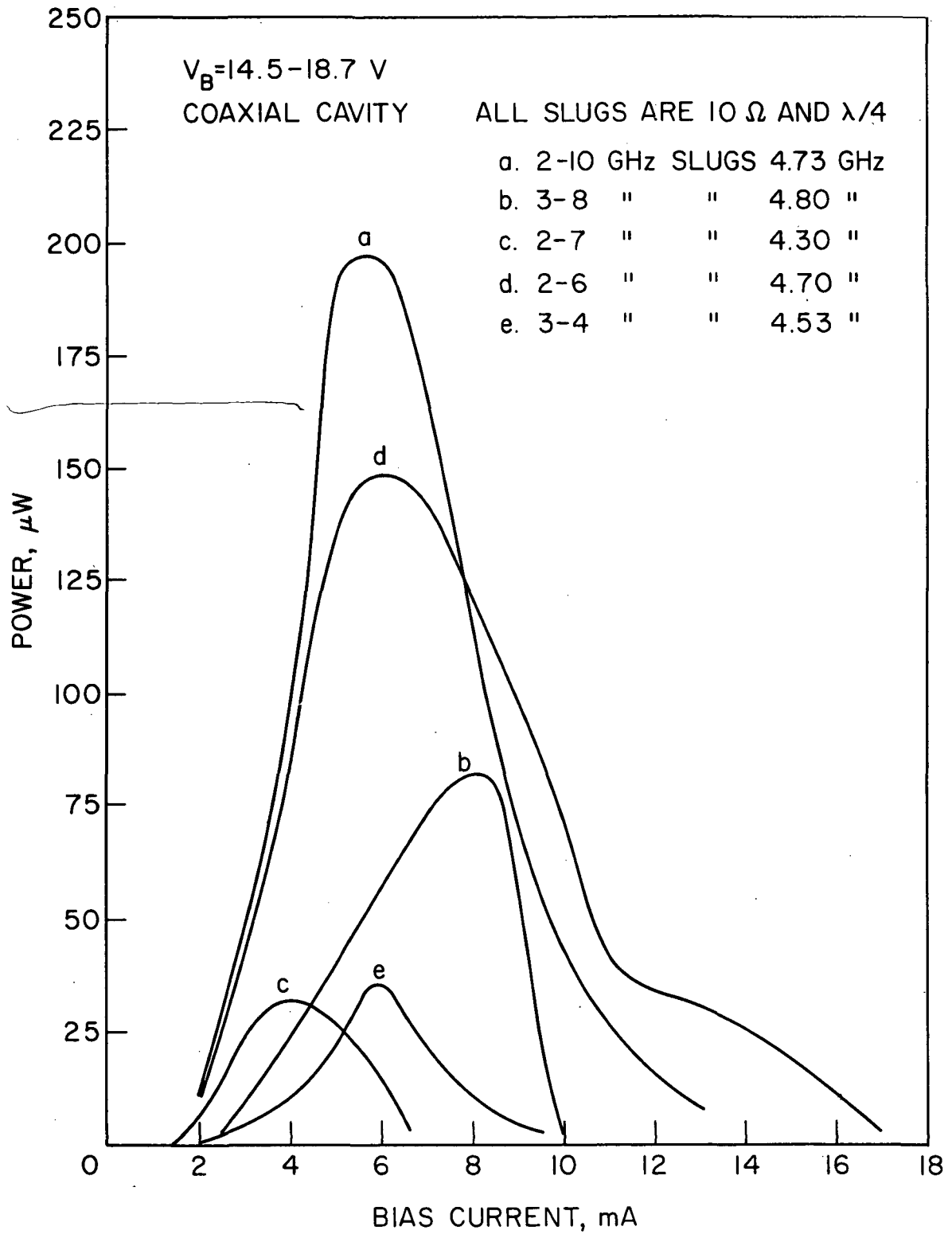FIG. 2.7 TYPICAL POWER OUTPUT VS. CURRENT OF PtSi-np$^+$ DIODES.

FIG. 2.8 TYPICAL POWER OUTPUT VS. CURRENT OF pnp$^+$ DIODES.
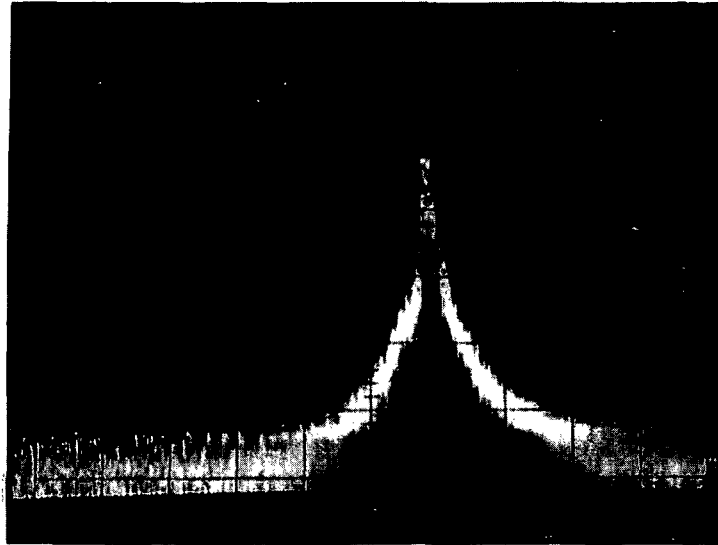
IF BANDWIDTH: I kHz

IF GAIN: 70

LOG DISPLAY

SWEEP TIME: I s/cm

SPECTRUM WIDTH: 30 kHz/cm

FREQUENCY: 4.6 GHz

FIG. 2.9 FREQUENCY SPECTRUM OF A PtSi-np^{+} DIODE.

2.4 <u>Theoretical Characterization</u>. The small-signal properties of these devices and the characteristics of 50-Ω and 100-Ω coaxial cavities have been investigated. The results will be correlated to future measurements. A large-signal computer program is being developed and some numerical instabilities have been encountered and identified. It is hoped that these will be resolved shortly.

2.5 <u>Program for the Next Period</u>. The experimental and theoretical work on these devices will be continued. The development of the large-signal analysis for determining the capabilities of these devices will be continued.

3. Intermodulation Products in IMPATT Diode Amplifiers.

Supervisors: G. I. Haddad and N. A. Masnari

Staff: R. J. Trew

3.1 <u>Introduction</u>. The objective of this phase of the program is to determine the intermodulation characteristics of an IMPATT diode operated in a reflection amplifier circuit under multifrequency conditions. Measurements have been made of the intermodulation products generated when two equal-amplitude signals are applied to the input of an X-band IMPATT diode amplifier. The test results consist of measurements of amplifier output signals as a function of input signal power levels and frequency separations. The amplifier was tested over an input power range sufficient to fully saturate the device (i.e., reduce the maximum gain to less than 3 dB).

3.2 <u>Circuit Description</u>. The block diagram of Fig. 3.1 represents the basic reflection amplifier circuit used in these experiments. Input-output signal separation is provided by a coaxial three-port circulator. Amplifier tuning is accomplished through the positioning in the resonant cavity of two 20-Ω copper tuning slugs; one being $\lambda/4$ at 8 GHz, the other $\lambda/4$ at 10 GHz. The diode is located at the end of the resonant cavity and is kept at an

FIG. 3.1 REFLECTION AMPLIFIER CIRCUIT, TWO-FREQUENCY OPERATION.

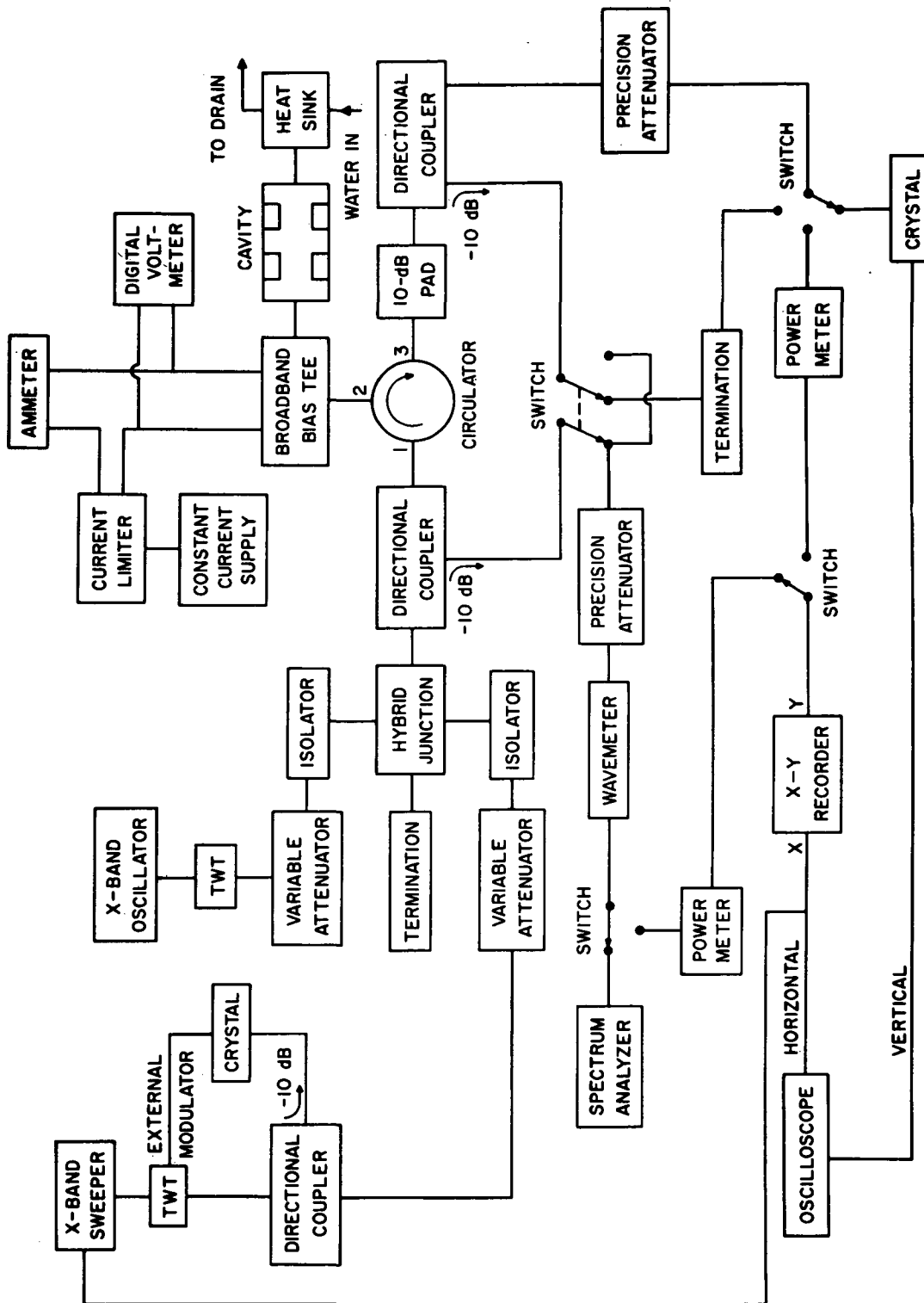approximately constant temperature by a water-cooled heat sink. The two source signals are amplified for large-signal operation and are introduced into the amplifier input through a "magic tee" that insures source signal isolation. The primary measurement circuit consists of a precision attenuator/spectrum analyzer combination calibrated to read power levels at the input-output plane of the resonant cavity. A cavity wavemeter is used to provide accurate signal frequency determination.

3.3 Results. Figure 3.2 illustrates the gain characteristics of the amplifier tuned to provide 20.4 dB of small-signal gain at a frequency of 9.340 GHz. Increasing the drive level results in a decrease in the maximum gain and its corresponding frequency. However, it is interesting to note that at frequencies below the maximum gain frequency it is possible to obtain increasing gain as a function of increasing drive level. The theoretical considerations for this behavior as well as the other basic operating characteristics of IMPATT amplifiers have been discussed elsewhere.[1,2] Increasing the drive level from small-signal operation to 200 mW of input power resulted in a decrease in maximum amplifier gain from 20.4 dB to 2.3 dB while the maximum gain frequency was shifting from 9.340 GHz to 8.910 GHz. During these experiments no spurious oscillations were observed at any drive level. The large-signal broadband behavior of IMPATT operation is also apparent as the 3-dB bandwidth increases from 55 MHz with small-signal operation to 545 MHz with 100 mW input power.

The intermodulation measurements consist of two sets of tests; one with an input signal (F_1) fixed at the frequency of maximum small-signal gain

1. Laton, R. W. and Haddad, G. I., "The Effects of Doping Profile on Reflection-Type IMPATT Diode Amplifiers," Proc. 1971 European Microwave Conf., Stockholm, Sweden, pp. A 5/1:1-A 5/1:4, August 1971.

2. Trew, R. J., Masnari, N. A. and Haddad, G. I., "Intermodulation Characteristics of X-Band IMPATT Amplifiers," To be presented at the 1972 IEEE-GMTT Int. Microwave Symp., Chicago, May 1972.
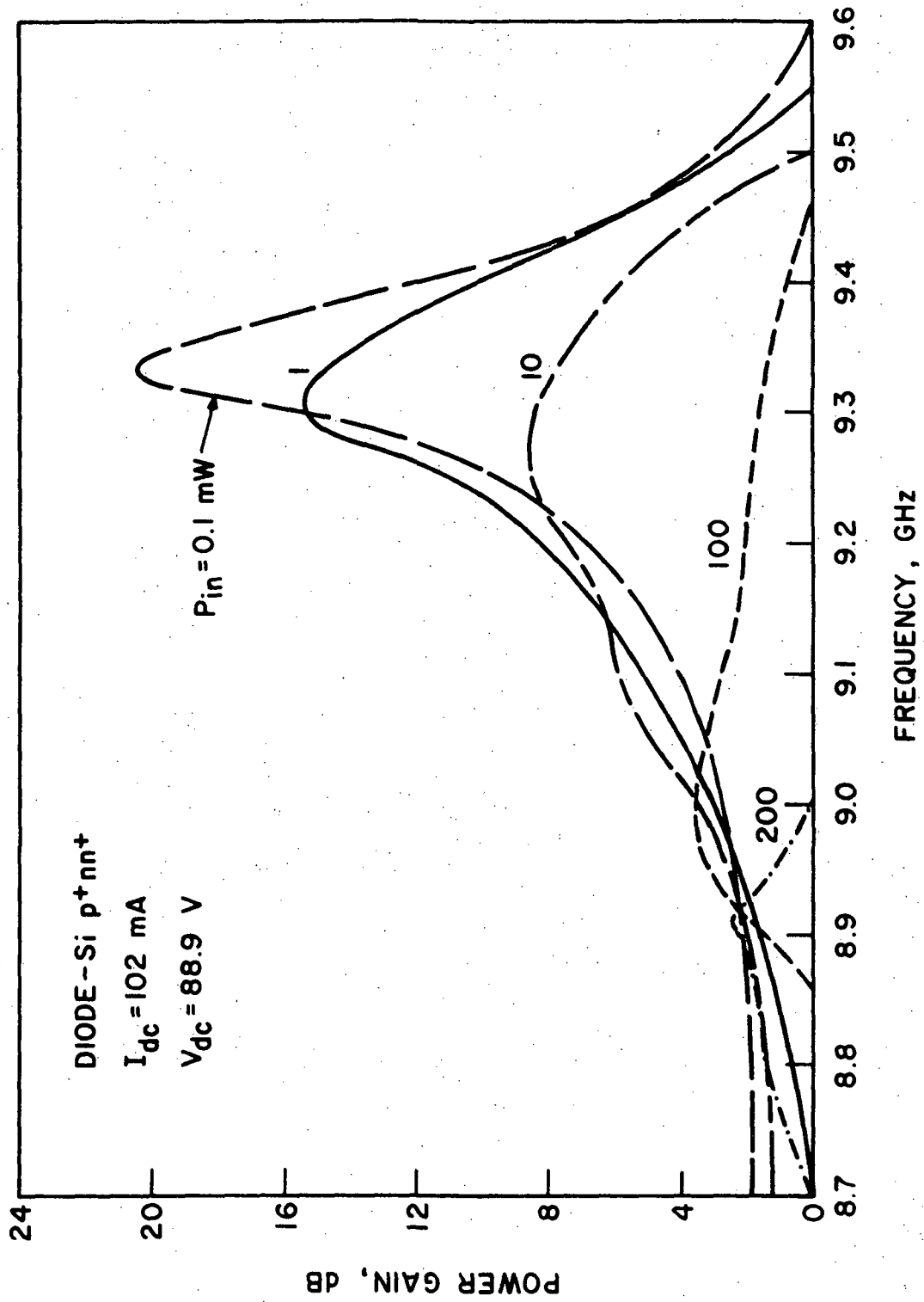
FIG. 3.2   IMPATT AMPLIFIER GAIN CHARACTERISTICS.

and the other input signal (F_2) set at higher frequencies defined by frequency separations of 3 MHz, 10 MHz, 30 MHz, 100 MHz and 200 MHz, and a second set of tests in which the input signal F_2 was fixed at the maximum small-signal gain frequency and F_1 was set at lower frequencies defined by the above frequency separations. Equal-amplitude input signals were used in all tests. Each test consisted of measurements of the amplifier output signals as a function of input drive levels first for single-frequency operation (only one input signal present at a time) and two-frequency (both input signals present) operation.

The $\Delta f = 3$ MHz test results of the first set of measurements are plotted in Fig. 3.3. At such small-frequency separations the gain is approximately constant and therefore the same output power is generated in both fundamental signals. Applying both signals simultaneously to the amplifier input resulted in the generation of a complete spectrum of signals in the amplifier output (Fig. 3.4). For this work the intermodulation signals are defined as follows. First order: $F_3 = 2F_1 - F_2$, $F_4 = 2F_2 - F_1$. Second order: $F_5 = 3F_1 - 2F_2$, $F_6 = 3F_2 - 2F_1$. Third order: $F_7 = 4F_1 - 3F_2$. As expected, the power generated in the output of the fundamental signals was less for two-frequency operation than for single-frequency operation. The power difference appeared as power at the intermodulation frequencies which have significant amplitudes even under small-signal operation. The first-order products F_3 and F_4 are the first to appear and have the same magnitude until high drive levels where the shift of the gain characteristics favoring amplification at lower frequencies becomes significant. At the higher drive levels F_3 is amplified more than F_4 due to the gain shift. This effect is more apparent at the higher-order intermodulation frequencies where the low-frequency product is always larger than its corresponding order high-frequency counterpart. However, for $\Delta f = 3$ MHz operation, the largest intermodulation product F_3 is always at least 12 dB down from the fundamental signals.
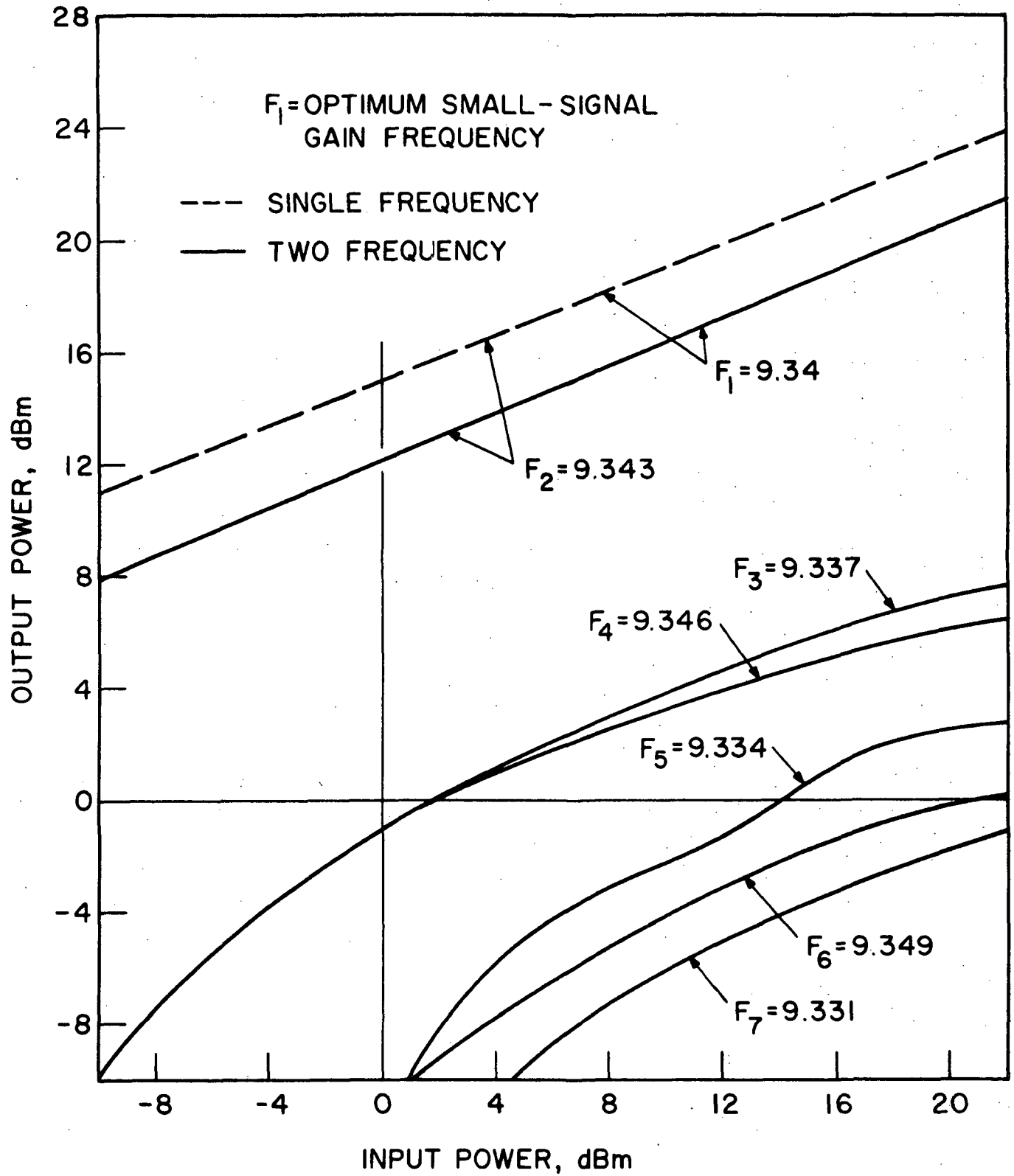
FIG. 3.3 DYNAMIC CHARACTERISTICS FOR IMPATT AMPLIFIER, TWO EQUAL-AMPLITUDE INPUT SIGNALS. (Δf = 3 MHz)
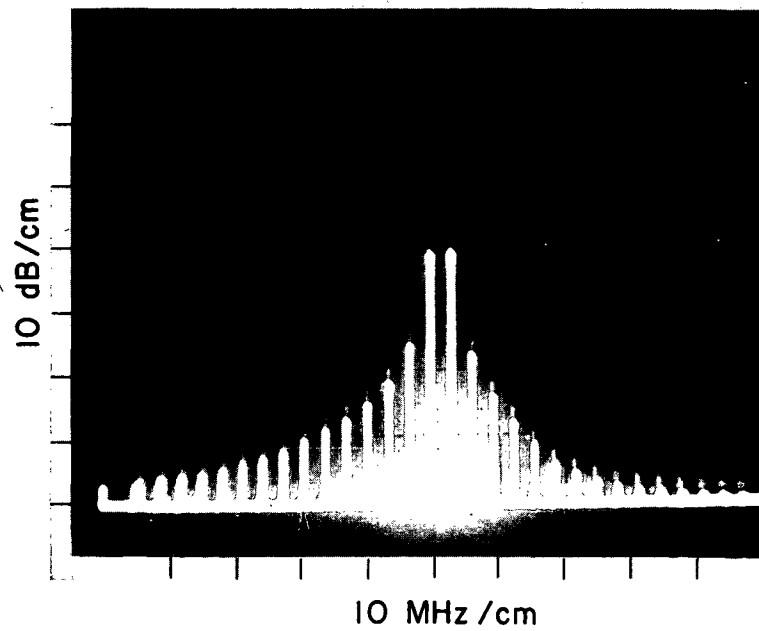
FIG. 3.4   OUTPUT SPECTRUM FOR IMPATT AMPLIFIER WITH TWO EQUAL-AMPLITUDE INPUT

SIGNALS. $(P_1 = P_2 = 100$ mW$)$

Increasing the input signal separation to 10 MHz (Fig. 3.5) results in the input signals no longer experiencing the same gain. The signal F_1 is always amplified more than F_2 although the two signals approach the same magnitude in the high drive level limit. This behavior is similar for both single-frequency and two-frequency operation and also holds for all frequency separations independent of their location relative to the gain characteristics. This result is expected due to the broadband nature of the gain characteristics at high drive levels. In the $\Delta f = 10$ MHz test, F_3 is always the largest intermodulation product attaining a value within 10 dB of F_2. The low-frequency dominance mechanism is apparent in the higher-order intermodulation products where the second-order low-frequency product F_5 is equal to the first-order high-frequency product F_4, and F_7 is always greater than F_6. When the frequency separation is increased to 30 MHz (Fig. 3.6), it is observed that the high-frequency fundamental signal F_2 loses proportionately more power to the intermodulation products than the low-frequency fundamental signal F_1. This occurs because the gain shift to low frequencies with increasing drive level partially compensates for power lost to the intermodulation products by the low-frequency fundamental. In this test the first-, second- and third-order low-frequency products are larger than the first-order high-frequency product with F_3 attaining a magnitude at one point within 7 dB of F_2. Figure 3.7 shows the results of the $\Delta f = 100$ MHz test. At this frequency separation interaction between the two fundamental signals has decreased such that there are fewer intermodulation products generated. The low-frequency fundamental signal shows identical output power under single-frequency and two-frequency operation until higher drive levels are reached. The high-frequency fundamental signal F_2, however, because it experiences lower gain, generates considerably less power than signal F_1 and shows a power difference in the single-frequency and two-frequency results over the entire input

FIG. 3.5 DYNAMIC CHARACTERISTICS FOR IMPATT AMPLIFIER, TWO EQUAL-AMPLITUDE INPUT SIGNALS. (Δf = 10 MHz)

FIG. 3.6 DYNAMIC CHARACTERISTICS FOR IMPATT AMPLIFIER, TWO EQUAL-AMPLITUDE
INPUT SIGNALS. ($\Delta f = 30$ MHz)

FIG. 3.7 DYNAMIC CHARACTERISTICS FOR IMPATT AMPLIFIER, TWO EQUAL-AMPLITUDE INPUT SIGNALS. (Δf = 100 MHz)

power range. It is interesting to note that the gain of the two-frequency F_2 signal changes from a positive value to a negative value at an intermediate input power level, whereas the corresponding single-frequency gain is positive at all levels. The only significant intermodulation products generated are the low-frequency signals F_3, which at one point is within 7 dB of F_2, and F_5. Increasing the frequency separation to 200 MHz (Fig. 3.8) results in little interaction between the fundamental signals. The low-frequency signal F_1 shows identical single-frequency and two-frequency results. The only significant intermodulation signal to be generated, F_3, appears to obtain all its power at the expense of F_2 and attains a magnitude within 2 dB of that signal. No amplification is present at the F_2 frequency, however, as the gain of the F_2 signal is always negative.

When signal F_2 is set at the maximum small-signal gain frequency and the tests are repeated for different frequency values of F_1, the only significant difference observed in the $\Delta f = 3$ MHz test from that already discussed is that the intermodulation signals have greater magnitudes under small-signal operation. The greater magnitudes result from the peak gain shifting from the F_2 frequency through the F_1 and lower-order intermodulation frequencies with increasing drive level. Due to the small frequency separations (3 MHz) this occurs under small-signal operating conditions.

Increasing the frequency separation to 10 MHz (Fig. 3.9) again results in constant gain with the fundamental signals F_1 and F_2 both generating the same output power. Low-frequency dominance, however, is apparent with the low-frequency intermodulation products generally being larger in magnitude than their high-frequency counterparts. The $\Delta f = 30$ MHz test (Fig. 3.10) clearly demonstrates the low-frequency dominance mechanism. Referring to the single-frequency curves, it is seen that first F_2 and then F_1 have the greatest output magnitude. This behavior is explained by the shift in gain
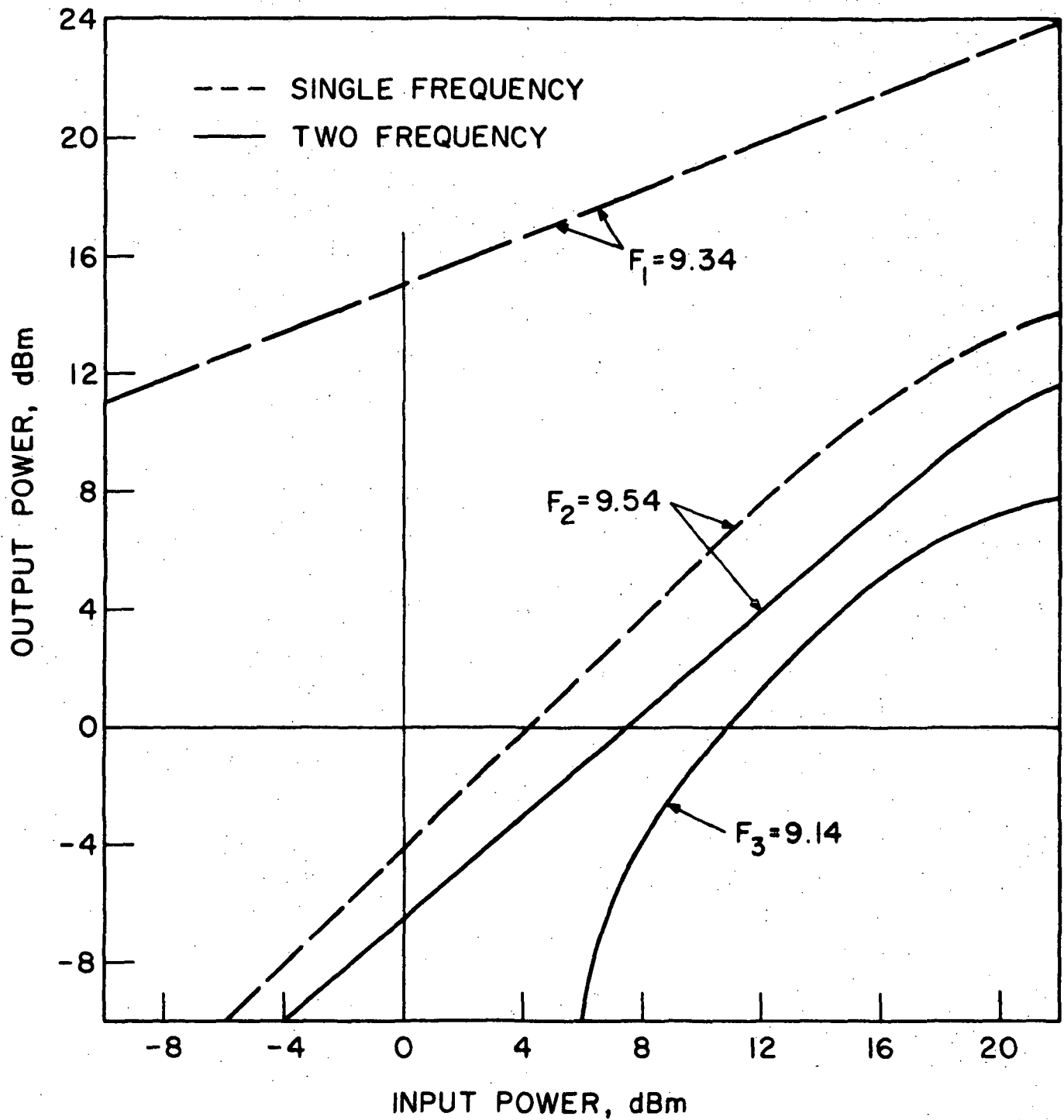
FIG. 3.8 DYNAMIC CHARACTERISTICS FOR IMPATT AMPLIFIER, TWO EQUAL-AMPLITUDE
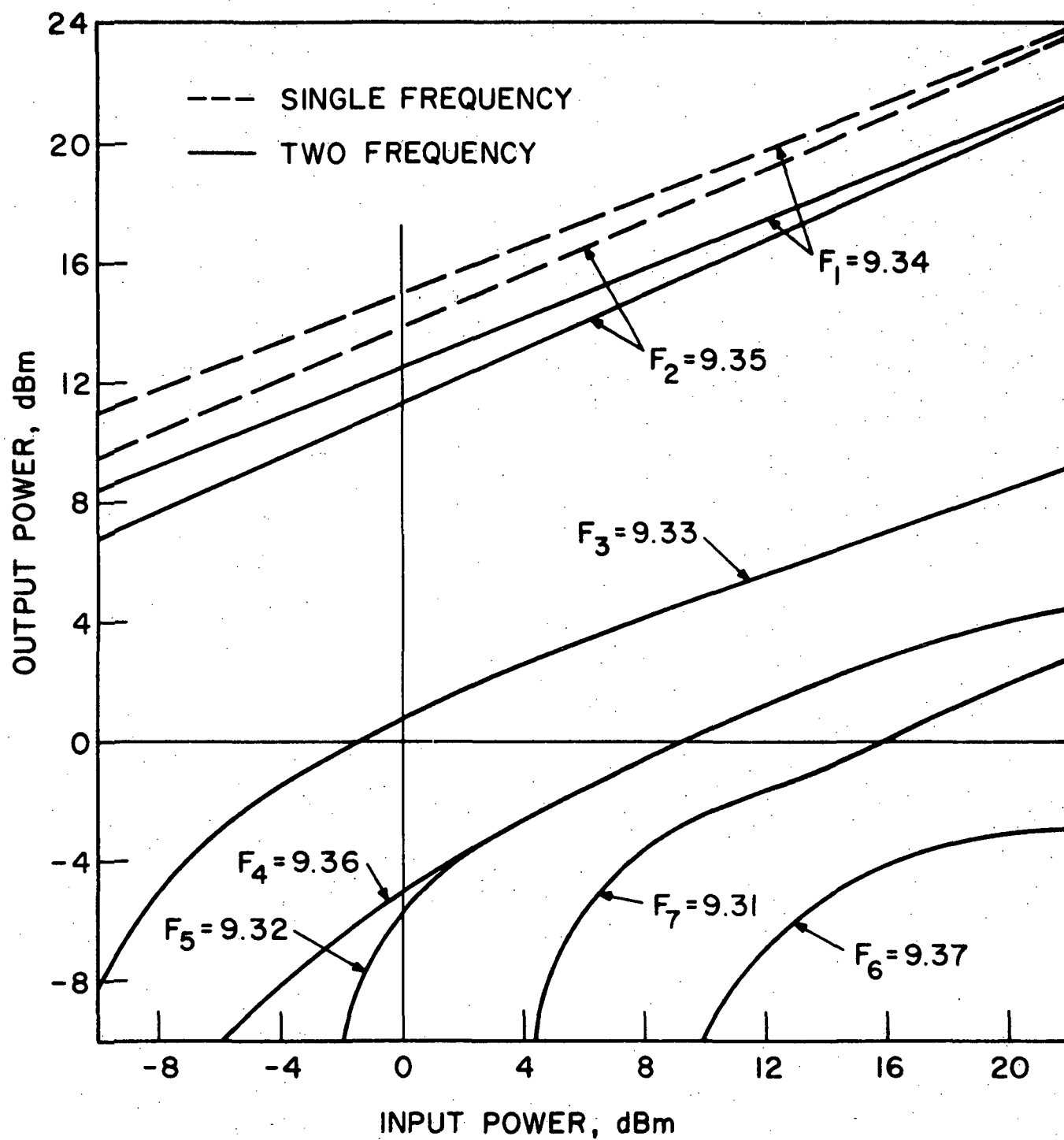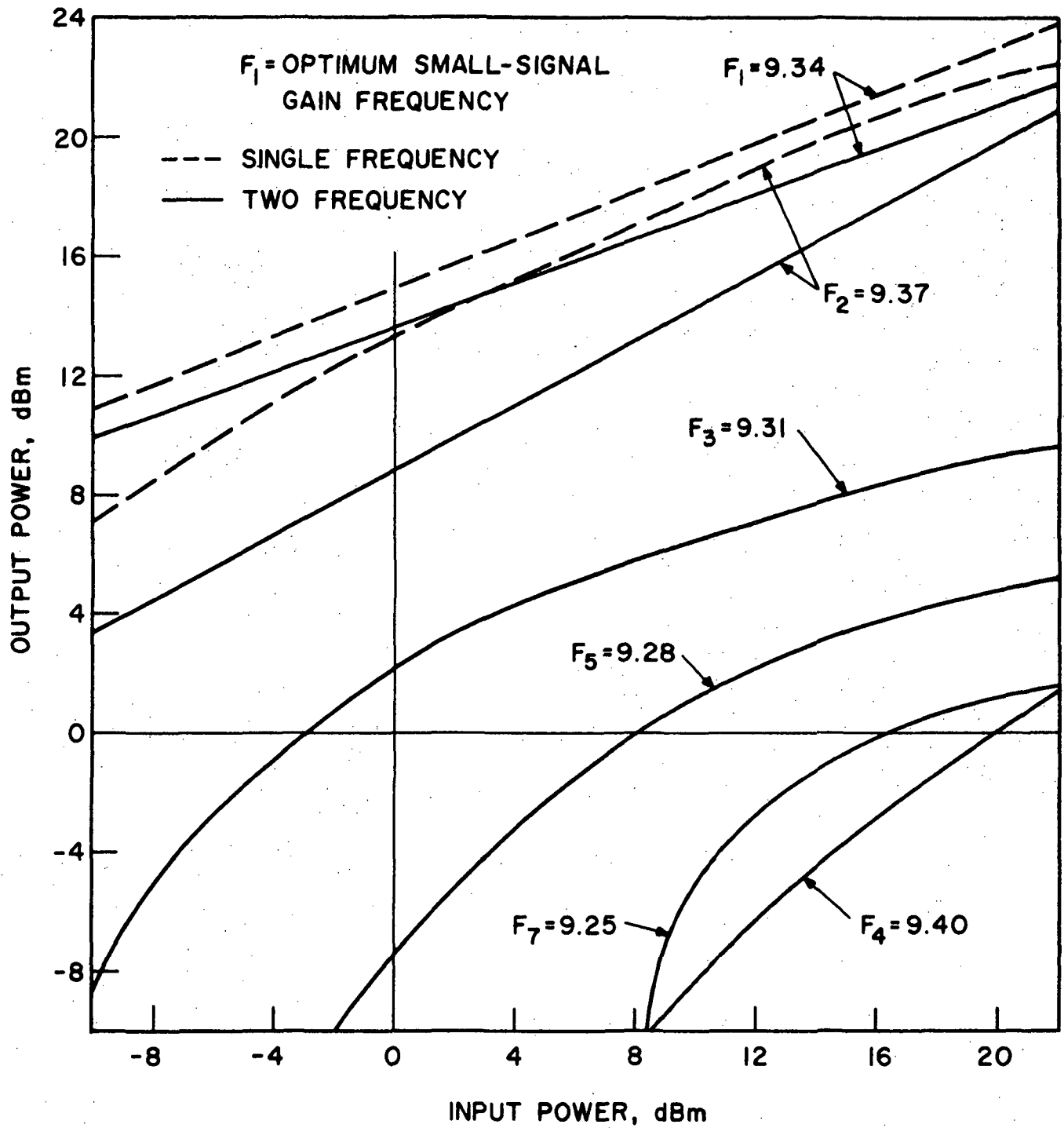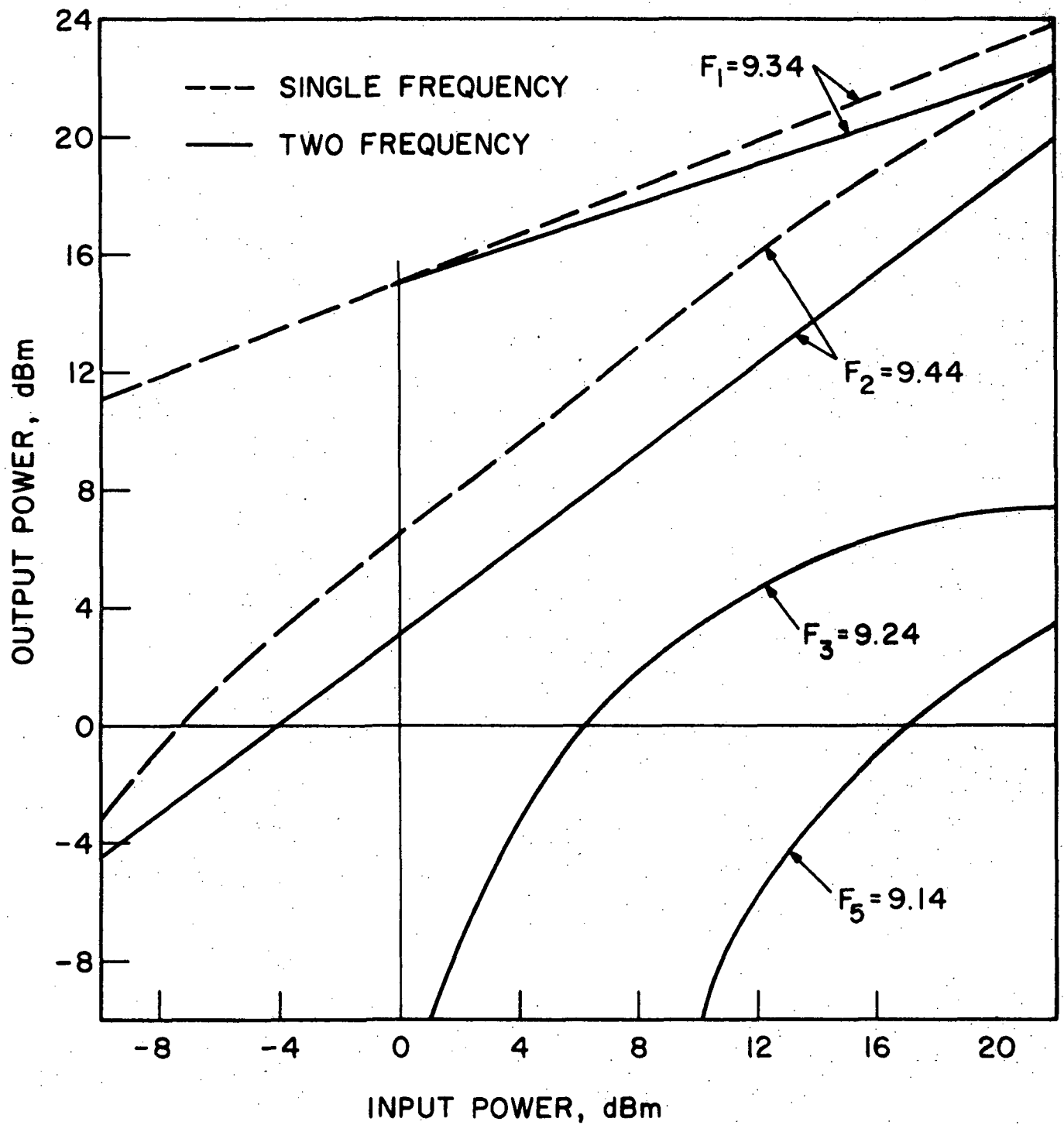
INPUT SIGNALS. (Δf = 200 MHz)
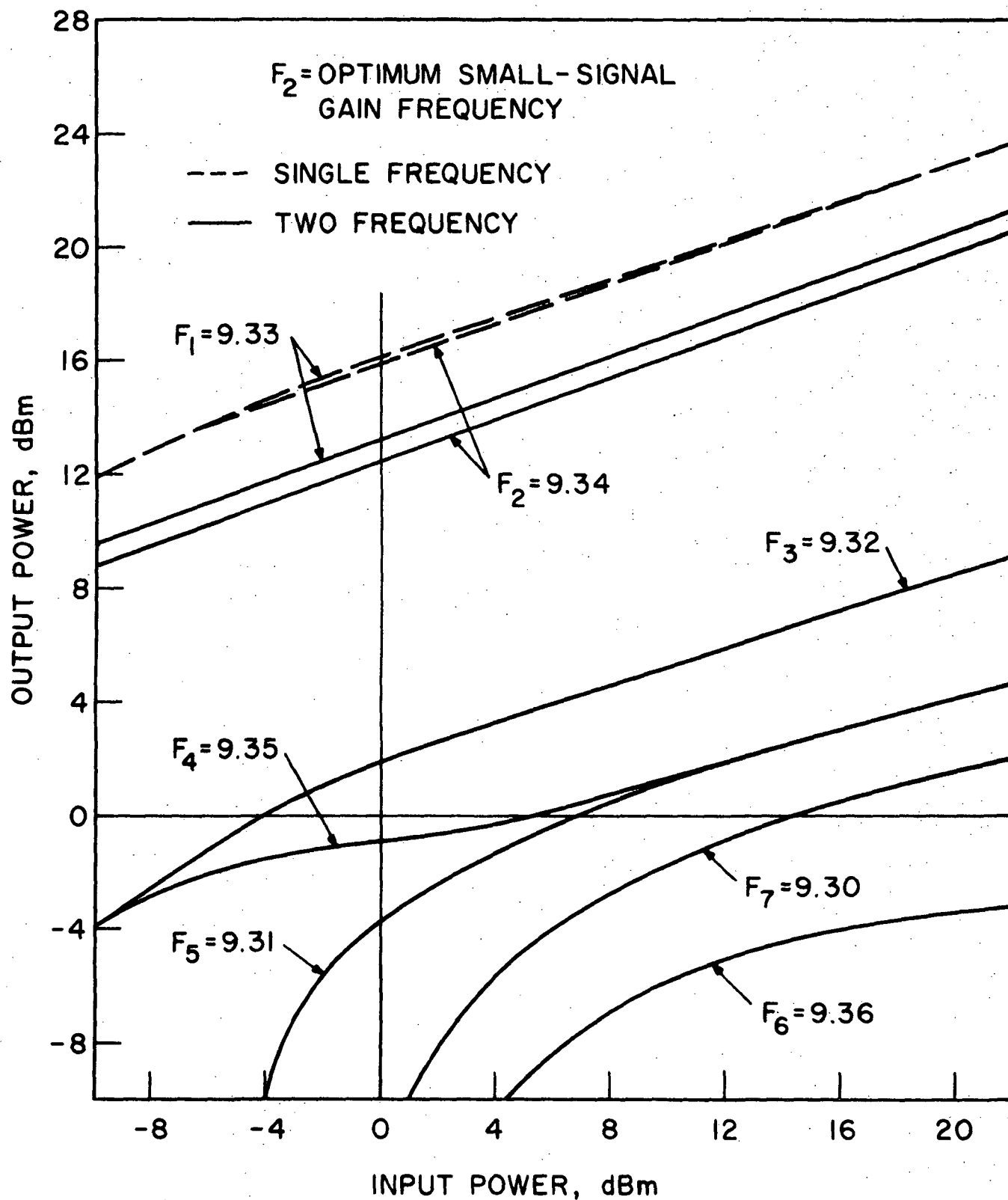
FIG. 3.9 DYNAMIC CHARACTERISTICS FOR IMPATT AMPLIFIER, TWO EQUAL-AMPLITUDE

INPUT SIGNALS. (Δf = 10 MHz)
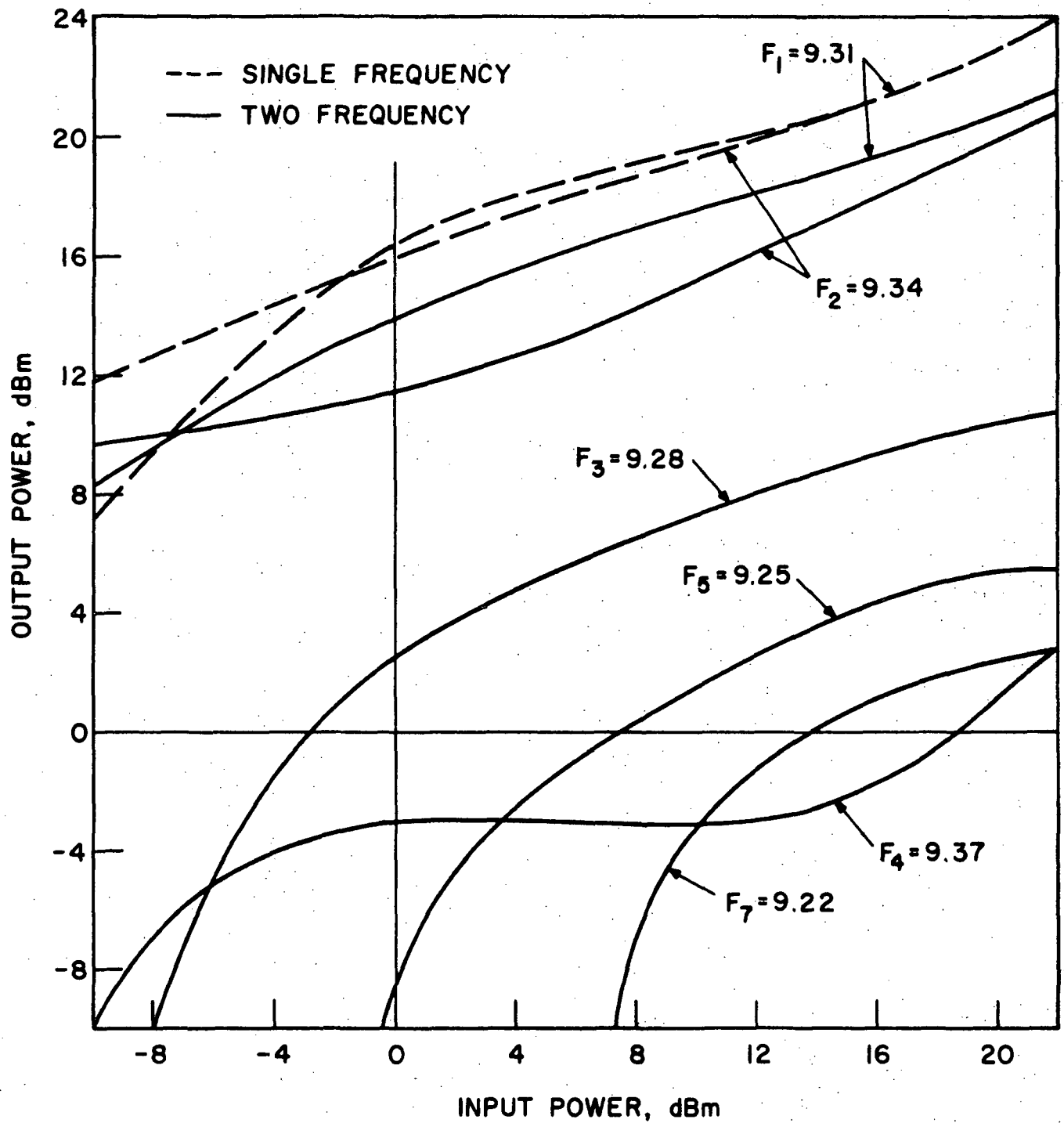
FIG. 3.10 DYNAMIC CHARACTERISTICS FOR IMPATT AMPLIFIER, TWO EQUAL-AMPLITUDE INPUT SIGNALS. (Δf = 30 MHz)

characteristics with increasing drive level. Since F_2 is fixed at the maximum

small-signal gain frequency, it initially generates the greatest output power.

However, as the drive level is increased the peak gain frequency is lowered and

passes through the F_1 frequency. As this occurs the greatest output power is

generated in F_1 and the F_1 and F_2 curves cross over. Increasing the drive

level further results in equal output power generated in the two signals as the

large-signal broadband behavior of the amplifier dominates. The two-frequency

results indicate that the crossover of the F_1 and F_2 curves occurs at lower

input power levels than the single-frequency results. This is due to the

proportionately greater loss of power to the intermodulation products

experienced by F_2. Since F_2 is initially the largest fundamental signal, F_4 is

the first intermodulation product to appear. However, as the peak gain shifts

through the low-frequency signals with increasing drive level F_3, F_5 and F_7 all

become larger than F_4. Increasing the frequency separation to 100 MHz

(Fig. 3.11) reveals that it is possible for the output power of one of the

fundamental signals to actually decrease as the input drive level is increased.

This is due to the increasing gain with increasing drive level present at the

frequencies below the maximum small-signal gain frequency (Fig. 3.2). The

relatively strong amplification of the low-frequency intermodulation signals

requires significant power transferral from the fundamental signals. Due to

the gain shift, the high-frequency signal F_2 experiences a rapidly decreasing

gain with increasing drive level whereas the low-frequency fundamental and

intermodulation signals all experience an increasing gain and then a slowly

decreasing gain as the drive level is increased. Therefore, the high-frequency

fundamental F_2 supplies most of the power generated at the intermodulation

frequencies and the result is a decrease in the output power of F_2 with

increasing drive level over a portion of the operating range. The $\Delta f = 200$ MHz

test (Fig. 3.12) again indicates decreasing interaction between the two
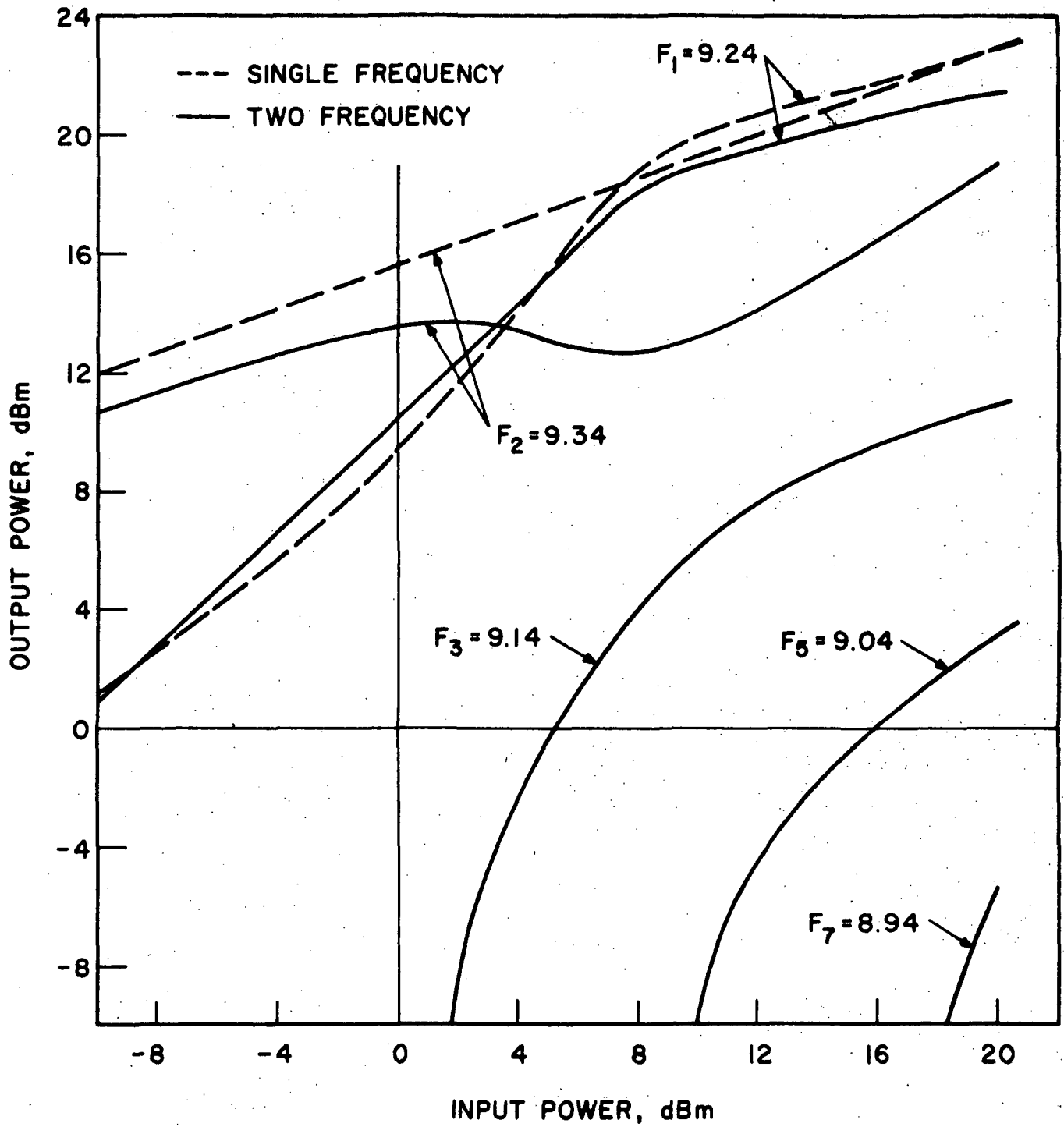
FIG. 3.11 DYNAMIC CHARACTERISTICS FOR IMPATT AMPLIFIER, TWO EQUAL-AMPLITUDE
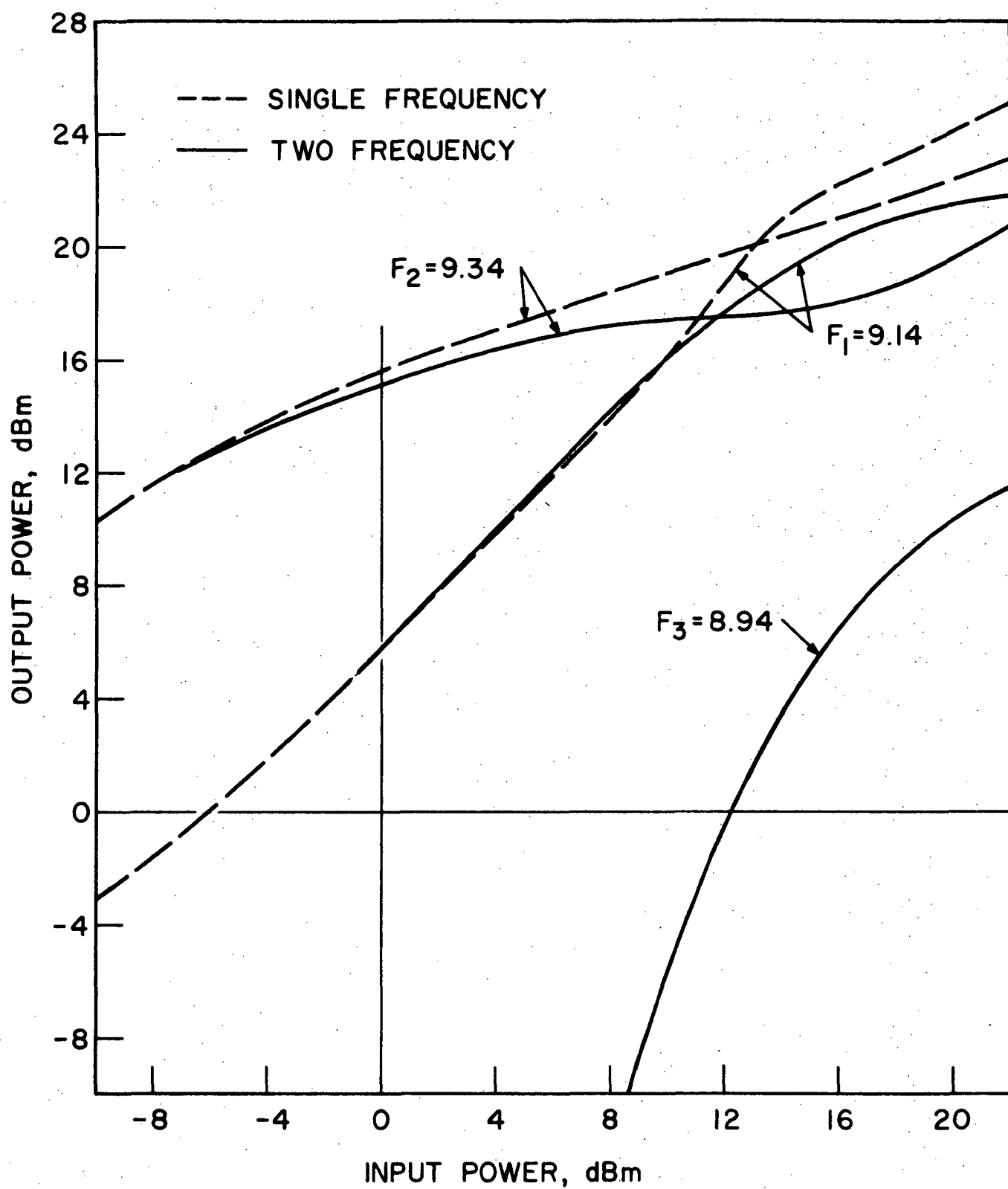INPUT SIGNALS. (Δf = 100 MHz)

FIG. 3.12 DYNAMIC CHARACTERISTICS FOR IMPATT AMPLIFIER, TWO EQUAL-AMPLITUDE

INPUT SIGNALS. (Δf = 200 MHz)

fundamental signals. Output power crossover is present although at a greater
input drive level than the preceding tests and higher drive levels are
required before a significant intermodulation product (F_3) is generated.
When F_3 appears it shows a rapid generation of output power reaching a level
within 8 dB of F_2.

3.4 Conclusions. Multisignal operation of IMPATT amplifiers results
in the loss of available output power at the fundamental signals with the
power difference appearing in signals at intermodulation frequencies. IMPATT
amplifiers are characterized by a decrease in the maximum gain and its
corresponding frequency with increasing drive level providing a low-frequency
dominance mechanism in which the low-frequency signals are amplified more
than the high-frequency signals. The magnitude of the intermodulation signals
is dependent to a greater extent upon the location of the signals relative to
the amplifier gain characteristics than upon the frequency difference between
the fundamental signals. It is possible for the first-, second-, and
third-order low-frequency intermodulation products to have a greater magnitude
than the first-order high-frequency product. Depending upon the location
of the signals relative to the amplifier gain characteristics it is possible
for the largest intermodulation product F_3 to attain a magnitude within 2 dB
of the smallest fundamental signal. Increasing the frequency separation
between the fundamental signals results in less interaction between them such
that there are fewer intermodulation products generated.

4. Harmonic Generation Using Read-Diode Varactors

Supervisor: G. I. Haddad

Staff: K. K. Dutta Choudhury

4.1 Introduction. The mathematical formulation of the C-V characteristic of the Read diode and its possible application as a harmonic generator were presented in Semiannual Progress Report No. 9. The theoretical small- and large-signal second-harmonic conversion efficiency and normalized power output of a Read diode and some commercially available punch-through varactors were presented in Semiannual Progress Report No. 10. In this report the measurements of the following parameters of the Read and some other types of diodes are presented:

1. The quality factor "Q" to estimate the cut-off frequency ω_c.

2. Series resistance R_s and its variation with bias voltage. The Read-diode series resistance is highly dependent on the bias voltage near the punch-through voltage.

4.2 Measurement of Quality Factor Q. The variation of capacitance with voltage is given by

$$C(V) = C_{vo}(\varphi - V_a)^{-\gamma} .$$

(4.1)

Assuming a circuit model[1] as shown in Fig. 4.1 for a mounted varactor, the input admittance at any arbitrary reference plane is given by

$$Y_{in} = \frac{1}{n^2} \left[jB_p + G_p + \frac{1}{(R_s + R) + j\left(X - \frac{1}{2\pi f C(V)}\right)} \right]$$

$$= G(V) + jB(V) ,$$

(4.2)

---

1. Roe, J. M., "Varactor Q Measurement," IEEE Trans. on Microwave Theory and Techniques (Correspondence), vol. MTT-19, No. 8, pp. 728-729, August 1971.
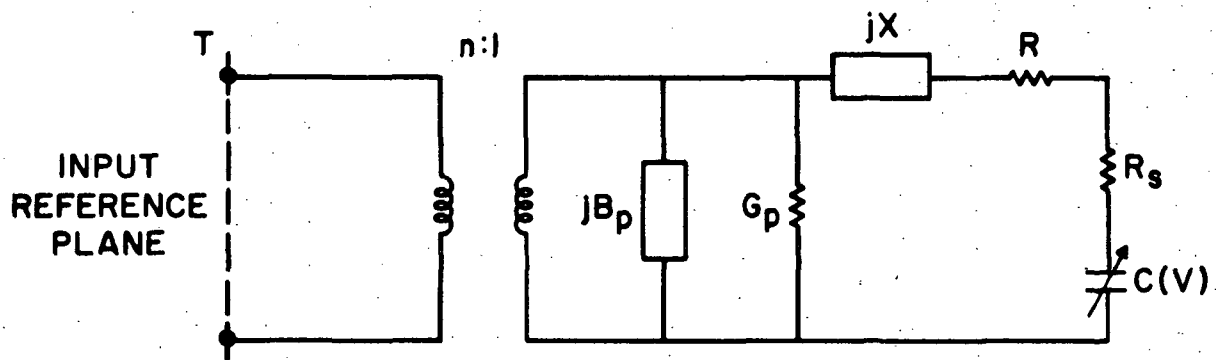
FIG. 4.1 CIRCUIT MODEL OF MOUNTED VARACTOR DIODE.

where

$$G(V) = \frac{1}{n^2} \left[G_p + \frac{R_s + R}{(R_s + R)^2 + \left(X - \frac{1}{2\pi f C(V)} \right)^2} \right] \quad (4.3a)$$

and

$$B(V) = \frac{1}{n^2} \left[B_p - \frac{X - 1/2\pi f C(V)}{(R_s + R)^2 + \left(X - \frac{1}{2\pi f C(V)} \right)^2} \right] . \quad (4.3b)$$

The locus of the input admittance on a Smith chart is a circle when $C(V)$ is varied by changing the bias voltage.

The shunt susceptance B_p vanishes when the reference plane is chosen so that the center of the admittance circle lies on the real axis. When $B_p = 0$, Eqs. 4.3a and b can be combined to yield

$$\frac{X}{R_s + R} - \frac{1}{2\pi f (R_s + R) C(V)} = \frac{B(V)}{\frac{G_p}{n^2} - G(V)} \quad (4.4)$$

or

$$Q_c - Q_k (\varphi - V_a)^{\gamma} = \frac{B(V)}{\frac{G_p}{n^2} - G(V)} , \quad (4.5)$$

where

$$Q_c = \frac{X}{R_s + R}$$

and

$$Q_k = \frac{1}{2\pi f (R_s + R) C_{vo}} .$$

The quantity Q_k determines the quality factor Q of the diode at any bias voltage.

The term G_p/n^2 is the minimum normalized admittance of the circuit and can be recognized as the intercept of the admittance circle with the real axis of the Smith chart.

4.3 <u>Experimental Procedure and Data Analysis</u>. The diode was mounted in a coaxial line as shown in Fig. 4.2.   After setting up the equipment shown in Fig. 4.3 at a particular frequency, the values of the following parameters were tabulated:

Bias voltage, V_a,

VSWR, S,

Position of 3-dB points for VSWR > 10, D_1 and D_2,

Position of minimum, D_{min},

Guide wavelength, λ_g.

The data were obtained for small changes of the applied bias.

Next the following steps were followed for determination of the quality factor from the measured data through a computer program.

1. The approximate normalized linear coordinates of the center and the radius of the impedance circle were determined by plotting the impedance data on a Smith chart. These values were used as initial values in the computer program.

2. The normalized input impedance at the reference plane S_{ref} was calculated at various bias voltages by using the formula

$$\bar{Z}_{in} = \frac{\bar{Z}_L + j \tan \beta \ell}{1 + j\bar{Z}_L \tan \beta \ell} \,, \qquad (4.6)$$

where $\bar{Z}_L$ = the normalized impedance at the reference plane S_{ref},

   $\bar{Z}_{in}$ = 1/S = the normalized input impedance at the position of the minimum,

   ℓ = the position of minimum minus the position of reference plane $(D_{min} - S_{ref})$,
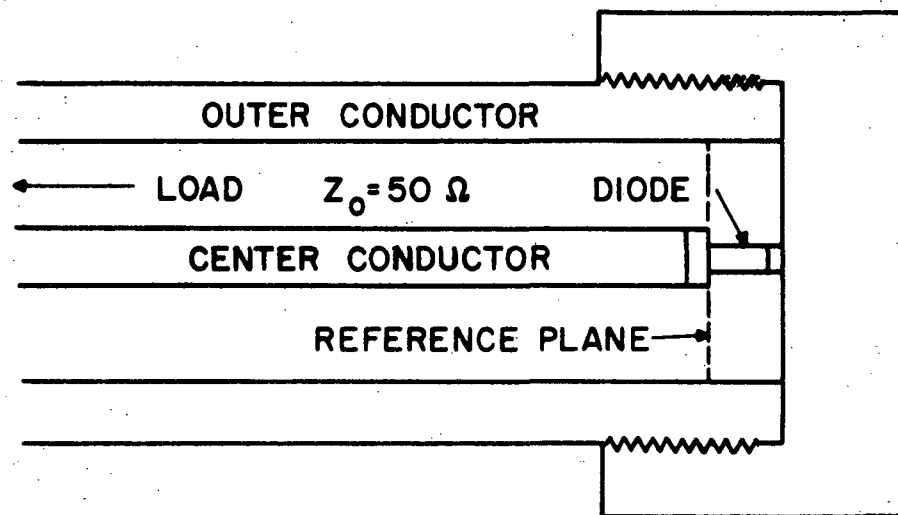
   β = $2\pi/\lambda_g$ and

FIG. 4.2 COAXIAL CIRCUIT.

FIG. 4.3 EXPERIMENTAL SETUP.

$$\bar{Z}_L = \bar{R}_L + j\bar{X}_L .$$ (4.7)

3. The impedance coordinates defined by Eq. 4.7 are converted to linear u-v coordinates on the Smith chart by the following conversion relationships:

$$u_n = 1 - \frac{2(\bar{R}_L + 1)}{\bar{X}_L^2 + (\bar{R}_L + 1)^2}$$ (4.8)

and

$$v_n = \frac{2\bar{X}_L}{\bar{X}_L^2 + (\bar{R}_L + 1)^2} .$$ (4.9)

4. The impedance circle is defined as

$$(u_n - u_o)^2 + (v_n - v_o)^2 = \rho_o^2 .$$ (4.10)

5. With the approximate values of u_o, v_o and ρ_o being known from Item 1, the corrected values are determined by iteration from the following relationships:

$$\rho_o = \frac{1}{N} \sum \sqrt{(u_n - u_o)^2 + (v_n - v_o)^2} ,$$ (4.11)

$$u_o = \frac{1}{N} \sum \left[u_n - \frac{\rho_o(u_n - u_o)}{\sqrt{(u_n - u_o)^2 + (v_n - v_o)^2}} \right]$$ (4.12)

and

$$v_o = \frac{1}{N} \sum \left[v_n - \frac{\rho_o(v_n - v_o)}{\sqrt{(u_n - u_o)^2 + (v_n - v_o)^2}} \right] .$$ (4.13)

The summation is over the total number of sets of data points N.

The distance of the center of the impedance circle from the origin is given by

$$r_o = \sqrt{(u_o^2 + v_o^2)} \ . \tag{4.14}$$

The u-coordinates at which the impedance circle intersects the real axis of the Smith chart is determined by addition and subtraction of ρ_o and r_o with the proper sign. These u-coordinates are converted to corresponding admittances. The minimum of these two values is used in place of G_p/n^2 in Eq. 4.5.

6. The center of the admittance circle is at a point diametrically opposite to the center of the impedance circle and is given by

$$u_o(\text{admit}) = -u_o(\text{imped}) \tag{4.15a}$$

and

$$v_o(\text{admit}) = -v_o(\text{imped}) \ . \tag{4.15b}$$

The orientation of the center of the admittance circle is given by

$$\tan \varphi = \frac{-v_o}{-u_o} = \frac{v_o}{u_o} \ . \tag{4.16}$$

The magnitude of the shift of the reference plane to a new reference plane to make the center of the admittance circle lie on the real axis is given by

$$D = (0.5 \times \lambda_g \times |\varphi|)/2\pi \ . \tag{4.17}$$

The sign of φ determines the direction of the shift of the reference plane S_{ref}.

7. The right-hand side of Eq. 4.5 is recalculated at the new reference plane at various bias voltages and are now defined as Q_m.

8. The values of Q_c and Q_k are determined by the method of least squares (assuming φ and γ to be known) by the following relationships:

$$Q_c = \frac{\frac{1}{N}\left[\sum Q_m - \dfrac{\sum^N (\varphi - V_a)^\gamma \times \sum Q_m(\varphi - V_a)^\gamma}{\sum^N (\varphi - V_a)^{2\gamma}}\right]}{\left[1 - \dfrac{\left[\sum (\varphi - V_a)^\gamma\right]^2}{N \sum (\varphi - V_a)^{2\gamma}}\right]} \tag{4.18}$$

and

$$Q_k = \frac{\left[\frac{1}{N}\sum^N Q_m \sum (\varphi - V_a)^\gamma - \sum Q_m(\varphi - V_a)^\gamma\right]}{\sum^N (\varphi - V_a)^{2\gamma}\left[1 - \dfrac{\left[\sum (\varphi - V_a)^\gamma\right]^2}{N \sum (\varphi - V_a)^{2\gamma}}\right]} . \tag{4.19}$$

These values of Q_c and Q_k are determined for various values of γ within a probable range. An error criterion is defined such that the average value of the square of the difference of the actual value of Q_m and the calculated value of Q_m is minimum. Then the value of Q_k for which this error is minimum is used for calculation of the quality factor at any bias.

4.4 <u>Experimental Results.</u> Table 4.1 gives the values of the quality factor Q and the value of series resistance of various diodes which were obtained by the method described previously.

Table 4.1

Determination of Quality Factor of Various Diodes

(Frequency = 7.5 GHz)

Diode Type	Q_k	V_a	Q	C(V) (pF)	R_s (Ω)
TI Read II	0.2154	0	0.2	6.5	16.36
TI Read I	0.3476	0	0.322	7.0	9.5
GD-2 (EPL)	4.242	75.0	36.6	0.3	1.9

Because of the nature of the C-V characteristic of Read diode II, only the portion (of the C-V characteristic) up to the punch-through voltage V_{pt} could be used in this method. This method cannot be used for studying the variation of series resistance with bias voltage, as the method uses the average value of resistance in the entire range for calculation of Q_k. The method described in the next section is used for studying the variation of series resistance R_s with bias voltage.

4.5 <u>Study of the Variation of Series Resistance of Diodes with Bias Voltage.</u> A diode package is shown in Fig. 4.4 and the equivalent circuit of a packaged diode at a reference plane between the ceramic and the flange of the diode is shown in Fig. 4.5. The following measurements were made to find the values of the elements of the equivalent circuit using the experimental setup of Fig. 4.3:
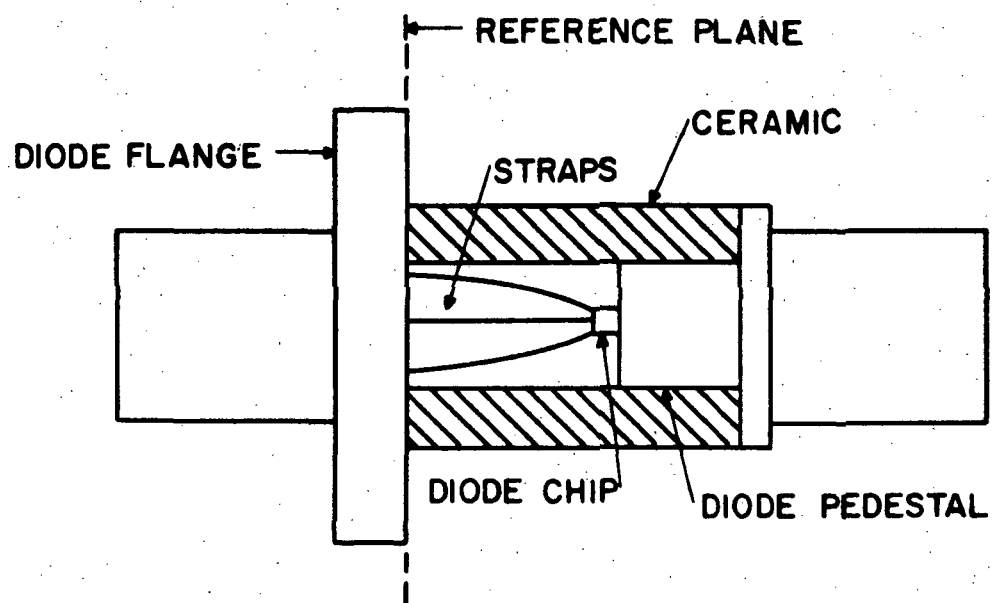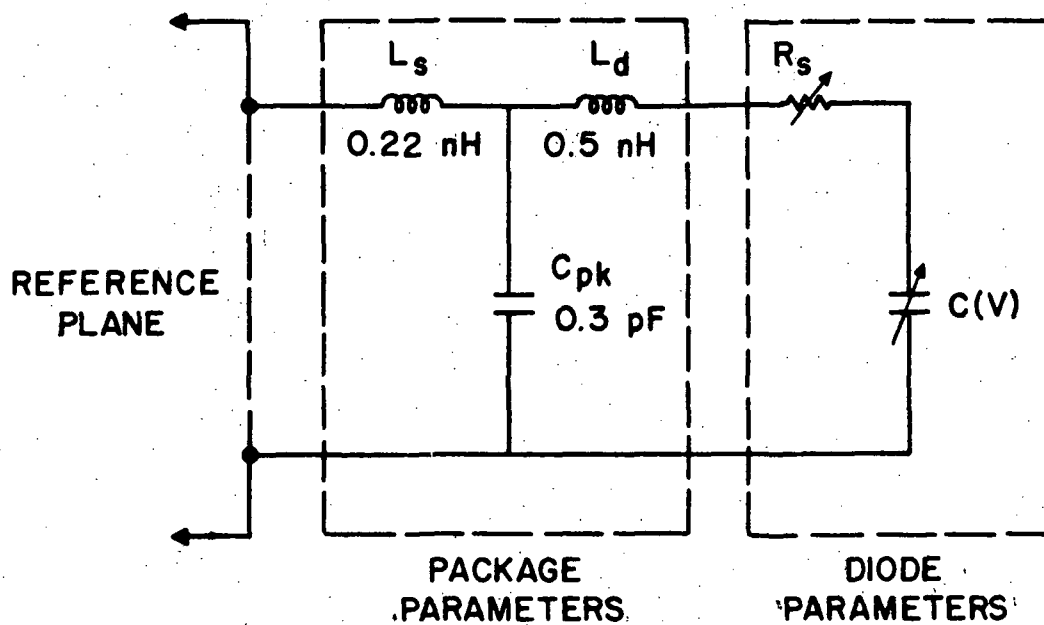
FIG. 4.4 DIODE PACKAGE.

FIG. 4.5 EQUIVALENT CIRCUIT OF THE DIODE PACKAGE AND CHIP.

1. Note the position of minimum and the corresponding VSWR at various frequencies of small intervals but a fixed bias voltage.

2. A shorting washer was used at the end of the diode mount to establish a reference plane. The positions of minima in the slotted line were noted at the frequencies used in Step 1. These positions of minima were shifted by the sum of the thickness of the washer and the flange of the diode to establish the reference plane at the desired location.

3. From the data of Steps 1 and 2 the impedance of the diode is calculated at various frequencies. A typical impedance plot is shown in Figs. 4.6 and 4.7.

4. The preceding steps are repeated at other bias voltages and for other types of diodes.

5. The values of the elements of the equivalent circuit were chosen to set the best agreement between the theoretical and experimental impedances. A computer program[2] performs the theoretical calculation of the impedance and makes a graphic presentation of the agreement between the experimental and theoretical results.

Once the correct values of the elements of the equivalent circuit are established, the same circuit is used at other bias voltages. Since the junction capacitance $C(V)$ is known at various bias voltages, a few runs of the computer program with different values of R_s can easily establish the correct values of R_s at that particular bias. The experimental results are tabulated in Table 4.2.

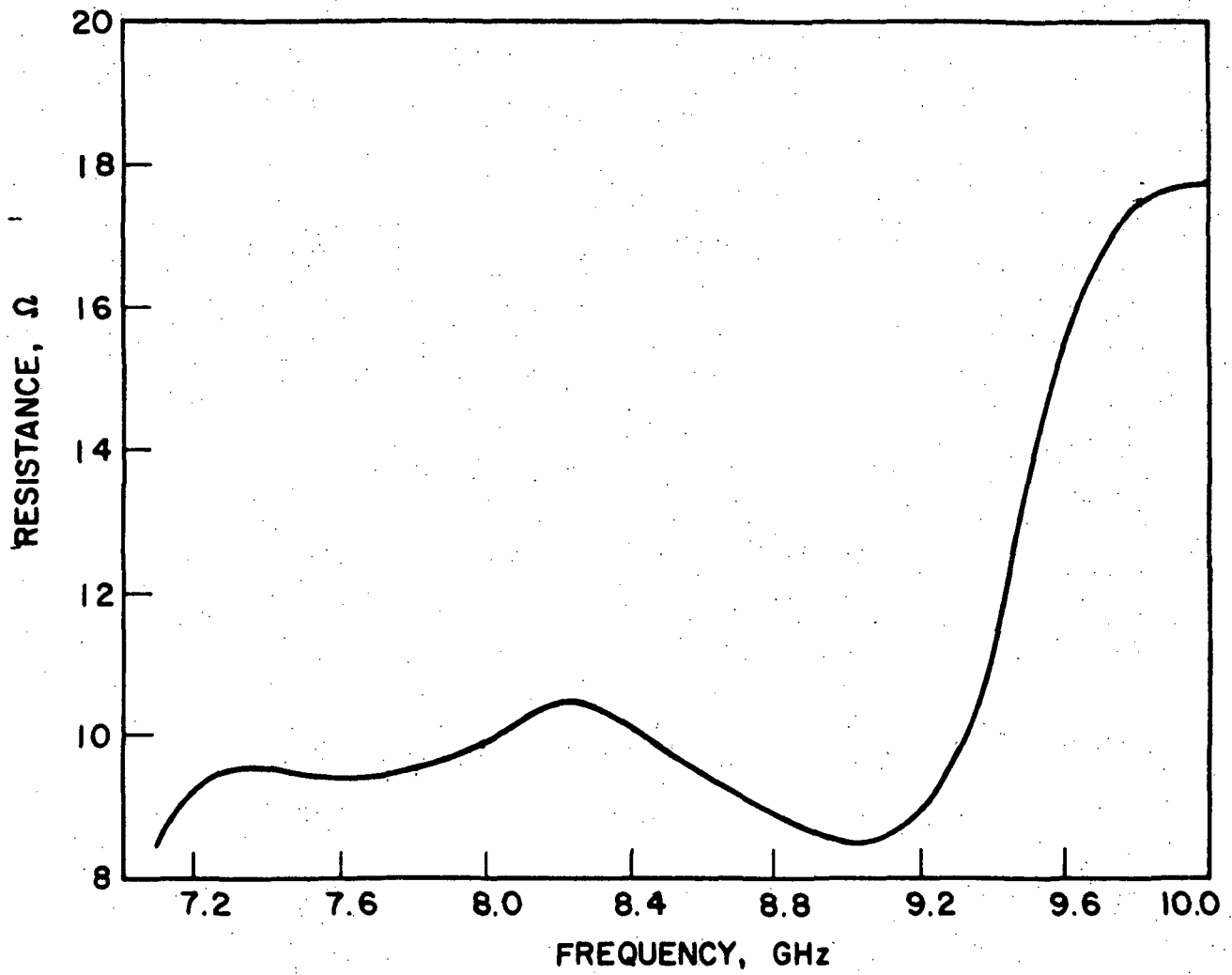2. Laton, R. W., private communication

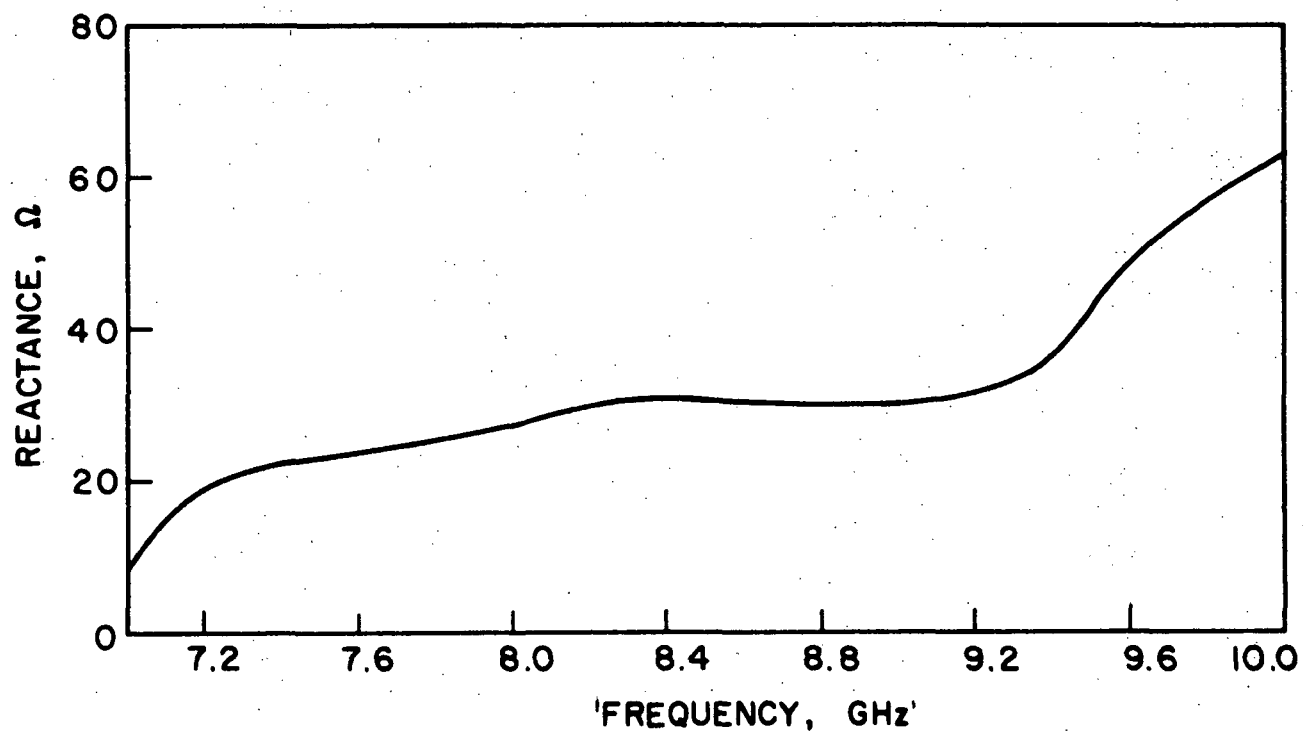FIG. 4.6 INPUT RESISTANCE OF TI READ DIODE I (PROCESSED HERE) AT BIAS = -30 V.

FIG. 4.7 INPUT REACTANCE OF TI READ DIODE I (PROCESSED HERE) AT BIAS = -30 V.

Table 4.2

Measured Values of R_s for Read Diodes

Diode Type	Bias Voltage V_a (V)	Series Resistance R_s (Ω)	Series Resistance R_s (Table 4.1) (Ω)	Punch-Through Voltage V_{pt} (V)
TI Read II	0	15.0	16.36	
TI Read II	-23	6.0		
TI Read II	-35	1.5		20
TI Read I (EPL)	0	10.0	9.5	
TI Read I (EPL)	-30	7.5		37.5
TI Read I (EPL)	-55	1.5		

4.6 Discussion. The Read diode because of its doping profile has a series resistance which is quite high before the punch-through voltage, decreases significantly after the punch-through voltage and is low and remains constant after the i-layer is completely swept out.

Because of the high series resistance when the bias voltage is below the punch-through voltage, the efficiency for harmonic generation will be decreased considerably at high-power operating levels. However, for efficient conversion at low power levels and for low-frequency harmonic generation the device may be quite useful. It will also be useful in voltage-tuning applications.

4.7 Program for the Next Period. Harmonic generation for low-level inputs utilizing a Read varactor will be investigated experimentally. The possibility of oscillator frequency tuning using this type of varactor will also be examined.